Advanced Fiber Materials (2024) 6:1343–1368
https://doi.org/10.1007/s42765-024-00454-0

REVIEW

Recent Advances in Functional Cellulose-Based Materials: Classification, Properties, and Applications

Yijia Deng[1] · Tianxue Zhu[2] · Yan Cheng[3] · Kaiying Zhao[4] · Zheyi Meng[5] · Jianying Huang[1] · Weilong Cai[1,6] · Yuekun Lai[1,6]

Received: 7 February 2024 / Accepted: 5 June 2024 / Published online: 26 June 2024

Abstract

Cellulose has sparked considerable interest in the advancement of biodegradable functional materials owing to its abundant natural sources and exceptional biocompatibility. This review offers a comprehensive review of the latest research and development concerning cellulose-based films, with a specific emphasis on their classification, properties, and applications. Specifically, this review classifies cellulose according to the various morphologies of cellulose (e.g., nanocrystals, nanospheres, and hollow ring cellulose) and cellulose derivatives (e.g., methyl cellulose, carboxymethyl cellulose, hydroxyethyl cellulose, and cellulose acetate). The subsequent section presents an analysis of cellulose-based films with improved mechanical properties, antibacterial characteristics, gas regulation, and hydrophobicity. A detailed discussion of the mechanisms that underlie these properties is provided. Additionally, representative applications of cellulosic composites, such as food packaging, medical supplies, and electronic devices, are summarized. Finally, the challenges faced by cellulosic materials are outlined, and a novel and feasible prospect is proposed to accelerate the future development of this material.

Keywords Cellulose-based film · Biocompatibility · Biodegradable materials · Multi-functional fiber · Electronic device

1 Introduction

Due to the increasing population and high energy demand, fossil fuels are being continuously utilized, resulting in various environmental and climate-related problems. Among these issues, "white pollution" from waste plastics presents a significant threat to the sustainable development of human society, and a crucial aspect of environmental governance. Cellulose, as a biodegradable material, is the most abundant and degradable biopolymer found on earth. The polymer chain is formed through the repeated connection of D-glucose, resulting in a highly ordered crystalline structure and scattered amorphous regions of nanosized linear polymers [1]. Subsequently, the formation of cellulose bundles, comprising cellulose nanofibers and microfibrils with diameters ranging from 10 to 100 nm, is facilitated through the aggregation of multiple cellulose chains, driven by hydrogen bonds and van der Waals forces. Given the inherent

Yijia Deng and Tianxue Zhu have contributed equally to this work.

✉ Yan Cheng
chengyan@ucas.ac.cn

✉ Jianying Huang
jyhuang@fzu.edu.cn

✉ Weilong Cai
wl.cai@fzu.edu.cn

✉ Yuekun Lai
yklai@fzu.edu.cn

[1] College of Chemical Engineering, Fuzhou University, Fuzhou 350116, People's Republic of China

[2] School of Materials and Chemistry, Anhui Agricultural University, Hefei 230036, People's Republic of China

[3] Zhejiang Engineering Research Center for Tissue Repair Materials, Joint Centre of Translational Medicine, Wenzhou Institute, University of Chinese Academy of Science, Wenzhou 325000, People's Republic of China

[4] Department of Materials Science and Engineering, Yonsei University, Seoul 03722, Korea

[5] State Key Laboratory for Modification of Chemical Fibers and Polymer Materials, Donghua University, Shanghai 201620, People's Republic of China

[6] Qingyuan Innovation Laboratory, Quanzhou 362801, People's Republic of China

structural composition of cellulose and its abundance of active groups, cellulose exhibits considerable potential for functional modification and demonstrates promising mechanical properties [2, 3]. The cellulose industry has achieved significant advancements in the development of nearly a hundred types of cellulose esters and ethers, with notable progress in researching their production processes and applications. The extensive utilization of cellulose and its derivatives across various sectors, including biomedicine, architectural coatings, food, petroleum, daily chemicals, new energy, ceramics, textiles, printing and dyeing, paper making, electronic components, environmental protection, liquid crystal displays, marine vessels, aerospace, and national defense, underscores the importance of advancing cellulose-based materials.

From the aspect of dimension and shape, cellulose can be subdivided into cellulose nanofiber (CNF) [4–8], spindle-like cellulose nanocrystals (CNCs) [9–12], micro-rod microcrystalline cellulose (MCC) [13, 14], anisotropic cellulose nanowhiskers (CNW) [15], bacterial cellulose (BC) secreted by bacteria with a high degree of purity [16], stackable two-dimensional nanosheets (CNS) [17, 18], cellulose nanospheres (s-NCs) [19], hollow annular cellulose nanocrystals (HTA-CNCs) etc. [20], which have been reported to show various benefits in cellulose used in value-added products. On the other hand, various functional cellulose derivatives were developed based on the substitution of hydroxy group in the cellulose chain, including semi-flexible cellulose ether derivative methyl cellulose (MC) [21, 22], water-soluble anionic surfactant carboxymethyl cellulose (CMC) [23, 24], ethyl cellulose (EC) (which shows water resistance, amphiphilic, high transparency and good flexibility, elastic deformation) [25–27], transparent degradable hydroxyethyl cellulose (HEC) [28, 29], thermo-responsive hydroxypropyl cellulose (HPC) [30–32], hydroxypropyl methyl cellulose (HPMC) [33], cellulose acetate (CA) with antibacterial performances, and water-resistant phosphorescent cellulose [34–37]. Various derivatives of cellulose have been used as adhesives or substrates in food packaging, coating materials, electronic products, and medical supplies.

This review highlights the latest advancements in cellulosic paper-based equipment utilized in food packaging, bioengineering supplies, and electrical equipment. First, we categorize and summarize cellulose and its derivatives based on functional groups and morphology. Subsequently, we delve into discussions regarding cellulosic paper-based composites showcasing enhancements in mechanical properties, antibacterial properties, gas regulation properties, hydrophobic properties, and other functionalities. The conventional applications of cellulosic paper-based composites across diverse domains, such as disposable plastic products, disposable tableware, food packaging and freshness-maintenance films, wound dressings, health-monitoring electronic devices, metal and oxide ion batteries, supercapacitors, and nanogenerators, are also extensively discussed (Fig. 1). Additionally, this review highlights the future challenges and prospects of value-added products based on cellulose and its derivatives.

2 Classification of Cellulose

2.1 Morphological Structure of Cellulose

Based on morphologies, cellulose can be divided into MCC [13], CNF [38], CNW [39], and CNS [40]. MCC is a non-fibrous, highly flowable porous crystalline particle with the size of micrometers, which can be extracted from plant cellulose after hydrolysis treatment. The polymer chains of microcrystalline cellulose (MCC) are densely packed in the crystalline region, whereas chemical and enzymatic interactions typically occur in the amorphous regions. CNF, a cellulosic material, is derived through mechanical processing of cellulosic suspensions, typically featuring a diameter ranging from 20 to 50 nm and a length spanning 500–2000 nm. On the other hand, CNW is produced through selective hydrolytic or oxidative degradation of the amorphous regions of cellulose using acids, enzymes, or oxidants, while preserving its crystalline regions. CNS showcases highly crystalline cellulose type II sheet-like nanostructures, characterized by nanometer-scale thickness and width, while extending to micrometer lengths.

CNC has been widely used as filler in composites in recent years due to its excellent physical, chemical, and ecological properties. CNC itself is a biomass organization, which has a natural affinity for composites and can form an "adaptive structure", which has the effect of weakening the local stress at the interface. In CNC composites, when subjected to stress, the CNC particles may slide along the surface of the filler material, and the broken bonds can rejoin, forming new bonds. This process helps to maintain a certain level of bonding strength between the matrix and the filler material, even in the presence of damage. Under stress, the CNC particles can slide along the surface of the filler material, and the broken bonds can reform into new ones. This process helps to maintain the bonding strength between the matrix and the filler material, thus reducing the degree of damage to the composite material. The incorporation of various forms of cellulose materials into the matrix allows for adjustment of mechanical properties, biodegradability, and loading of therapeutic agents within the composites. Consequently, composites containing different forms of CNC are extensively utilized across diverse fields including packaging, engineering plastics, 3D printing, biomedical engineering, and beyond.

CNCs are novel mechanically enhanced nanoparticles with Young's modulus in the range of 100–130 GPa [41],

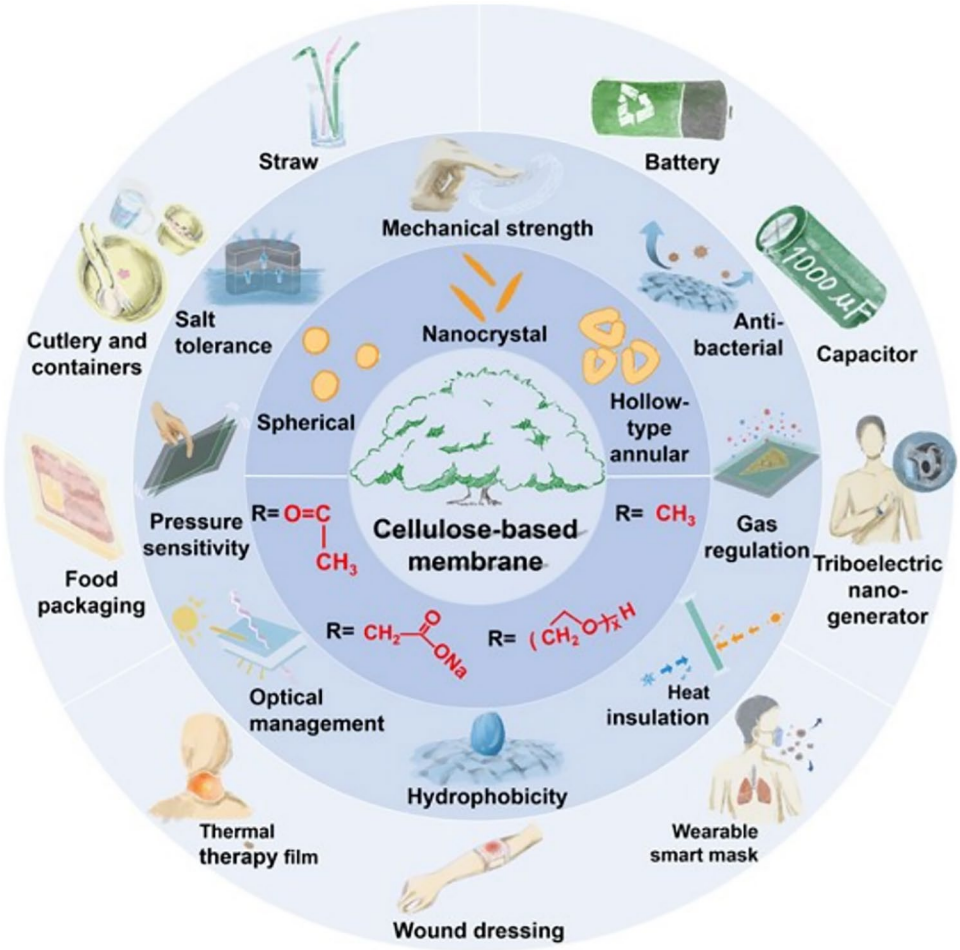

Fig. 1 The introduction of recent advances in applications for functional cellulose-based films

offering the advantages of low density (1.5–1.6 g/cm^3) [42], high strength (7500 MPa) [43]. Yang et al. applied a superhydrophilic CNC coating onto the surface, controlling its density using a composite intermediate adhesive layer. This innovative approach yielded a coating with universal and outstanding anti-fouling performance, effectively inhibiting oil adhesion, protein adsorption, and cell adhesion [12]. CNCs coatings adhere to the substrate and maintain structural integrity even when severely damaged. This provides a viable reinforcement method for dense, rigid materials.

In addition to the above commercially available cellulose morphologies, researchers have developed a wider variety of cellulose morphologies for different application scenarios. Patel et al. obtained rod-shaped CNCs and s-NCs through the treatment of acid hydrolysis and alizarin red staining thermal hydrolysis [44]. The average length of CNCs is 140 nm, while the diameter of s-NCs was 43 nm. Compared with ordinary sulfuric acid hydrolysis, SO_4^{2-} group, hydrogen sulfate ion (HSO_4^-), and hydrogen peroxide (H_2O_2) in APS thermal hydrolysis process are more active, which can penetrate deeper into the amorphous region inside the cellulose and accelerate the oxidation of hydroxy groups on the cellulose chain. The acidic environment caused by the hydrogen ions (H^+) will damage the 1,4-β glycosidic bond, leading to the depolymerization of cellulose and decreasing of cellulose nanospheres. CNCs with a hollow structure exhibit a superior specific surface area compared to the common cellulosic materials with rod-like and spherical structures. Consequently, CNCs with hollow structures present more opportunities for unique applications, serving as delivery carriers capable of loading a higher quantity of nanoparticles, drugs, and dyes. Xu et al. produced HTA-CNCs through ultrasonic treatment [20]. Throughout the processing, ultrasonic energy is encapsulated within minute yet protruding liquid bubbles, generating an ultrasonic field. Upon bubble collapse, a high-speed micro-jet with potent energy is produced, effectively disrupting the structural integrity of the cellulose chain. With prolonged treatment time, both inter- and intra-molecular hydrogen bonds progressively break down, resulting in a gradual decrease in the width of CNCs. Nanocellulose structures with larger specific surface areas exhibit promising potential for drug transport applications, and their distinctive loading properties are anticipated

to find broader utility in other realms of substance delivery as well.

2.2 Classification of Cellulose Derivatives

Cellulose is a polysaccharide comprised of cyclic D-glucopyranose units interconnected through a β-1,4-glycosidic bond, leading to alternating 180° rotations of the cellulose chain axes. The linear chain structure of cellulose comprises three reactive hydroxy groups, or OH groups, per anhydroglucose unit. This arrangement of –OH groups along its linear chain endows cellulose with a high degree of reactivity, facilitating easy esterification or etherification with chemical reagents. This has spurred the development of various cellulose derivatives, broadly classified into three categories: cellulose ethers, cellulose esters, and cellulose ether esters [45]. In addition to the chemical diversity offered by the -OH groups, the unique molecular structure of cellulose bestows upon it other properties, including chirality, hydrophilicity, and degradability.

Wang et al. reported a water-soluble cellulose nanocrystal@methylcellulose (CNC@MC) film-based bandage sensor. The cellulose nanocrystal was derived from recycled waste paper through the treatment of dissociation, hydrolysis, and dialysis (Fig. 2a) [21]. The presence of a broad fiber size distribution in pure CNC film leads to a propensity for agglomeration during film formation (Fig. 2b). Combined with the exceptional film-forming properties of MC, the CNC/MC composite film exhibits satisfactory flexibility and transparency, with the needle-shaped CNC evenly dispersed within the MC matrix (Fig. 2c). The results indicate that the water-soluble MC with good film-forming properties can stably disperse CNC in water.

As a typical cellulose ether derivative, CMC is an anionic hydrophilic polysaccharide. The negatively charged CMC aqueous solution can interact with multivalent cations and possess strong thickening and water retention ability. Compounding CMC with BC synthesized by microorganisms, Wu et al. prepared a novel BC-CMC film with both positive and negative charge to realize the conversion of osmotic energy by in-situ fermentation (Fig. 2d) [23]. Due to the presence of hydrogen bonds and electrostatic force, CMC macromolecules can adhere firmly to BC progenitor fibers, which is conducive to adjusting the size of the nanochannel in the film from the nanoscale to the microscale (Fig. 2e). In the BC-CMC film, a porous micro-structure is evident, with the pore size increasing with higher CMC content (Fig. 2f). The peak of FTIR spectrum for BC-CMC at 1731 cm^{-1} can be attributed to the conversion from hydroxy group to the carboxyl group [46], indicating the negative effect of the added CMC on the formation of hydrogen bonds between BC fibrils (Fig. 2g) [47].

HEC cellulose is a water-soluble, non-ionic cellulose derivative with three hydroxy groups on each benzene ring and rich in electron-donating groups. Compared to MC, HEC exhibited superior water retention, capacity, excellent flow regulation performance and abundant electron donor groups, which can be produced by the reaction of cellulose with ethylene oxide (C_2H_4O) under alkaline conditions (Fig. 2h). Dai et al. designed an omnidirectional wind energy harvester (OWEH) based on HEC thin films for wind vector sensing and environmental energy acquisition [28]. The visible light transmittance of the transparent HEC film is 91%, higher than that of ordinary cellulose film (Fig. 2i). The flexible HEC film can not only endure large folding and bending but also can fit on the surface of leaves with irregular lines (Fig. 2j). The high-performance HEC film enhances output efficiency by amplifying vibration frequency in OWEH. With an arithmetic mean roughness of approximately 23.34 nm, the film strengthens the bond between the cellulose base and friction material, resulting in further enhancement of the output capacity of electronic instruments (Fig. 2k). The –OH group of HEC appears narrower compared to cellulose, while the peaks corresponding to C–H and C–O–C bonding in HEC are more pronounced than those of the original cellulose (Fig. 2l), suggesting the partial conversion of hydroxy groups in HEC to hydroxyethyl. The environmentally friendly and biodegradable HEC film demonstrates excellent light transmittance and flexibility, rendering it promising for applications in self-powered sensing and monitoring within intelligent agricultural inspection systems.

Wang et al. combined CA with perovskite quantum dots ($CsPbX_3$) through electrospinning and ink-jet printing to realize photoluminescence color radiative cooling (PCRC), which achieves sub-ambient full-color radiative cooling (Fig. 2m) [35]. When sunlight is irradiated, the photoluminescent colorant on the top layer of PCRC absorbs photons and converts them to emit mid-infrared wavelengths. The sunlight projected to the bottom layer can be reversely emitted by the CA nanocellulose film, thus achieving heat radiation and cooling effect (Fig. 2n). Abundant hydroxy group in CA can form O–Pb bond with perovskite $CsPbX_3$ quantum dots, which further increases the stability of the latter (Fig. 2o). Through the electrospinning process, randomly stacked nanofiber CA films are created at the bottom layer, forming a disordered structure that effectively scatters sunlight, as depicted in Fig. 2p. In addition, $CsPbX_3$ quantum dots are uniformly distributed on CA films through ink-jet technology without obvious agglomeration, indicating that the randomly packed CA can effectively facilitate the dispersion of quantum dots and improve its quantum efficiency (Fig. 2q). CA can maximize the sunlight reflection of photoluminescent colorants, thereby minimizing the solar thermal effect in radiation cooling.

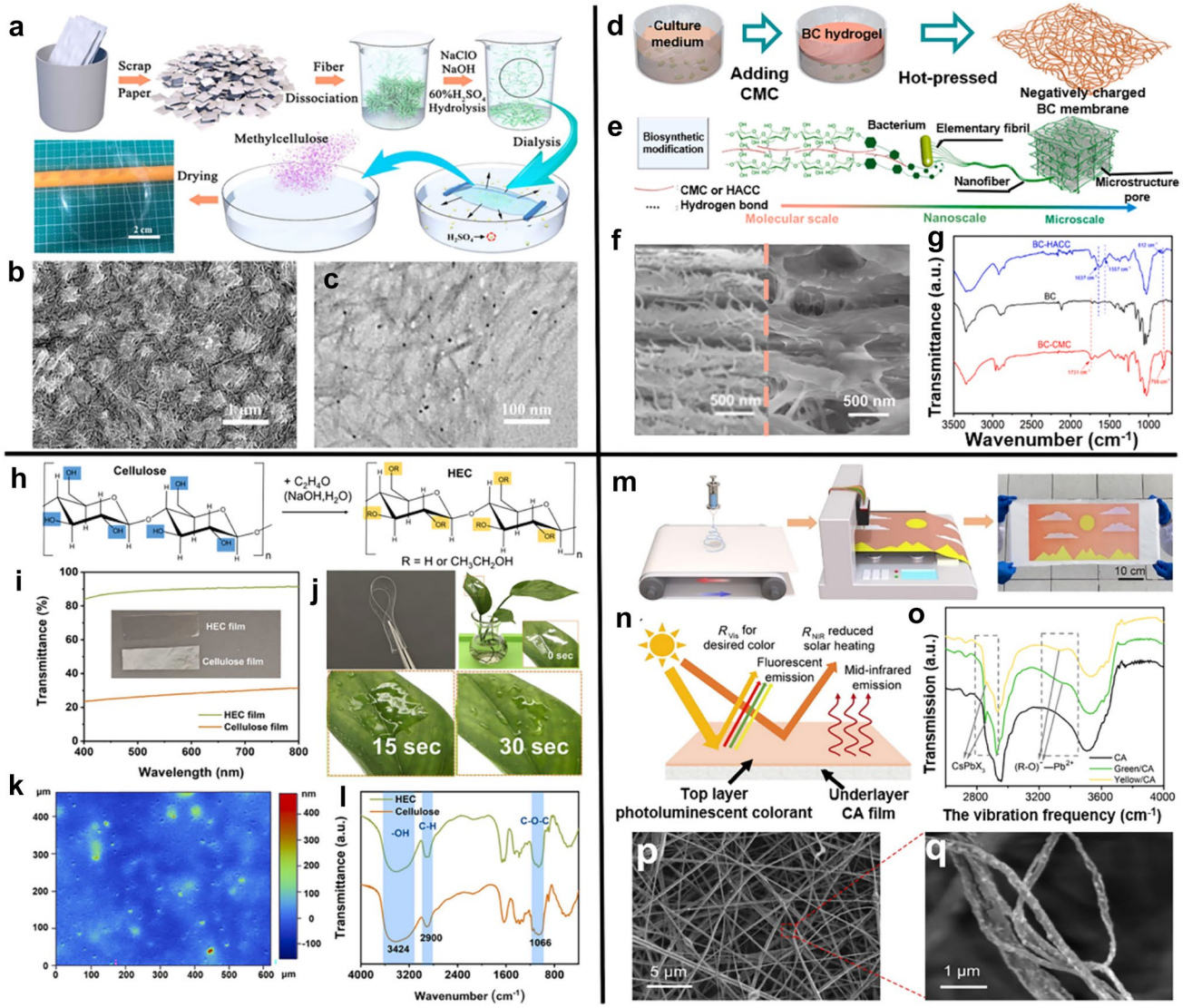

Fig. 2 **a** Preparation process of CNC@MC film, **b** high magnification SEM image of coarse fiber of wasted paper, **c** TEM image of CNC@MC; reproduced with permission from ref. [21], Copyright 2022, Elsevier. **d** Preparation of BC-CMC film, **e** schematic diagram of the nanochannels modified by CMC, **f** cross-sectional SEM images of BC-CMC_5 (left) and BC-CMC_{25} (right), **g** FTIR spectra of the native BC, BC-CMC, and BC-HACC films; reproduced with permission from ref. [23], Copyright 2021, Elsevier. **h** Synthesis route of HEC, **i** optical images and transmittance of HEC film and cellulose film, **j** flexibility of HEC film and its dissolution in deionized water spray, **k** Raman spectra of the HEC film, and **l** FTIR spectra of HEC film and cellulose film; reproduced with permission from ref. [28], Copyright 2022, Elsevier. **m** Schematic of the electrostatic-spinning setup for producing CA nanofibers film, **n** the radiation cooling principle of PCRC, **o** FTIR spectra of CA/$CsPbX_3$, and **p**, **q** SEM images of CA/$CsPbX_3$ fibers; reproduced with permission from ref. [35], Copyright 2022, Elsevier

Cellulose derivatives are formed by substituting the hydroxy groups of cellulose with various groups such as methyl, carboxymethyl, ethyl, hydroxyethyl, cyanoethyl, hydroxypropyl, and others under specific conditions. The degree of substitution of cellulose derivatives varies depending on the number of substitution positions. Altering the terminal groups of cellulose enhances its properties, making it suitable for diverse applications in different scenarios (Table 1). The mechanical strength values of various cellulose derivatives exhibit significant variation. Cellulose films with low tensile strength are suitable for use in flexible devices, conforming to different shapes of substrates. Cellulose films with slightly higher mechanical strength can serve as substitutes for plastic products. Most cellulose derivatives can be dissolved in low-toxicity organic solvents, and some of them can be solved with water.

Table 1 Published information on the properties and related applications of cellulose derivative materials

Cellulose derivative	Tensile strength (MPa)	Solubility	Biodegradability	Application	Ref.
MC	50	Water	Natural environment, 1 month	Triboelectric nanogenerator	[21]
CMC		Water		Osmotic energy harvesting	[23]
CMC	26.08 ± 6.7	Water	Soil burial, 1 month	Food packaging	[48]
EC	~ 38	Ethanol	Bacterial degradation	Edible conductor	[27]
HEC	~ 3.5	Water		Wind energy harvester	[28]
HEC	14.06 ± 3.0	Water	4 °C, aqueous environment, 6 days	Food packaging	[49]
CEC	~ 220	Acetone		Uranium filter film	[50]
CEC		Acetone	Soil burial, 19 days	Flexible transistor	[51]
HPC	0.56	Water		Triboelectric nanogenerator	[52]
HPC		Water	37 °C, PBS solution, 1 month	Hydrophobic mats	[53]
HPMC	5.0	Water		Self-powered sensor	[33]
HPMC		Water	Soil burial, 1 month	Food packaging	[54]
CA		Acetic acid		Radiative cooler	[35]
CA	62.0 ± 3.0	Acetone	Soil burial, 1 month	Biodegradable bag	[55]
CAB	21.57 ± 0.8	Acetone		Fiber bundle	[56]
CAB	0.94 ± 0.21	Acetone	37 °C, PBS solution, 2 weeks	Scaffold for tissue engineering	[57]

EC ethyl cellulose, *CEC* cyanoethyl cellulose, *HPMC* hydroxypropyl methyl cellulose, *CAB* cellulose acetate butyrate

3 Properties of Cellulose-Based Materials

3.1 Mechanical Property

Industries generate a substantial volume of plastic waste, and the breakdown of microplastics from it poses a serious threat to human health as they can be absorbed and accumulate in the body. Consequently, ongoing research on the development and utilization of biodegradable materials as substitutes for plastic has garnered widespread attention and sparked intense debate [58–60]. Yang et al. fabricated an edible BC-based straw through biosynthesis and rolling layer-by-layer structure, and the obtained sample showed excellent wet and dry mechanical strength [61]. The BC hydrogel can be obtained through the acetobacter xylosus enzymatically hydrolyzed carbon sources (such as glucose), and then the edible straw was prepared after rolling up and drying (Fig. 3a). Its unique 3D nanonetwork structure imbues it with high strength. To address the lack of hydrophilicity and adhesion of BC, a thin layer of sodium alginate (SA) was introduced onto the surface of the BC film. Calcium lactate was utilized as a cross-linking agent to mitigate mechanical and adhesion issues (Fig. 3b, c). The tensile strength of BC/SA straws is (420.5 ± 31.3) MPa, which is much higher than that of commercial paper straws (with a tensile strength of (40.8 ± 5.5) MPa). The modulus of BC-related products is higher than that of paper straws, indicating that BC straws possess high rigidity and are not easily deformed (Fig. 3d). The wet tensile strength of the BC/SA straw reaches 110 MPa, while the wet stress–strain curve of the paper straw indicates that it has become a flexible material (Fig. 3e). The bending strength of BC-based straw is three times greater than paper straw, up to (35.3 ± 3.9) MPa, which is expected to meet the requirements of practical applications (Fig. 3f). Furthermore, after being coated with SA, numerous fibers in BC establish a stable structure with SA. SA can form a cross-linked network with cellulose through hydrogen bonding, facilitating stress dispersion and enhancing the mechanical strength of BC/SA composite films (Fig. 3g). As a high-performance edible material, BC meets the standards of material safety and sustainable development, holding significant potential for replacing disposable plastics.

In response to the demands of modern manufacturing fields, such as food processing, pharmaceutical manufacturing, aerospace, and electronic applications, there is a widespread pursuit of lightweight and strong structural materials. Many materials with excellent mechanical properties have been developed from petroleum products, but most of them necessitate high-cost manufacturing processes. Bamboo is an excellent biomimetic structural material with lightweight and strong properties [62, 63]. Li et al. reported a top–down

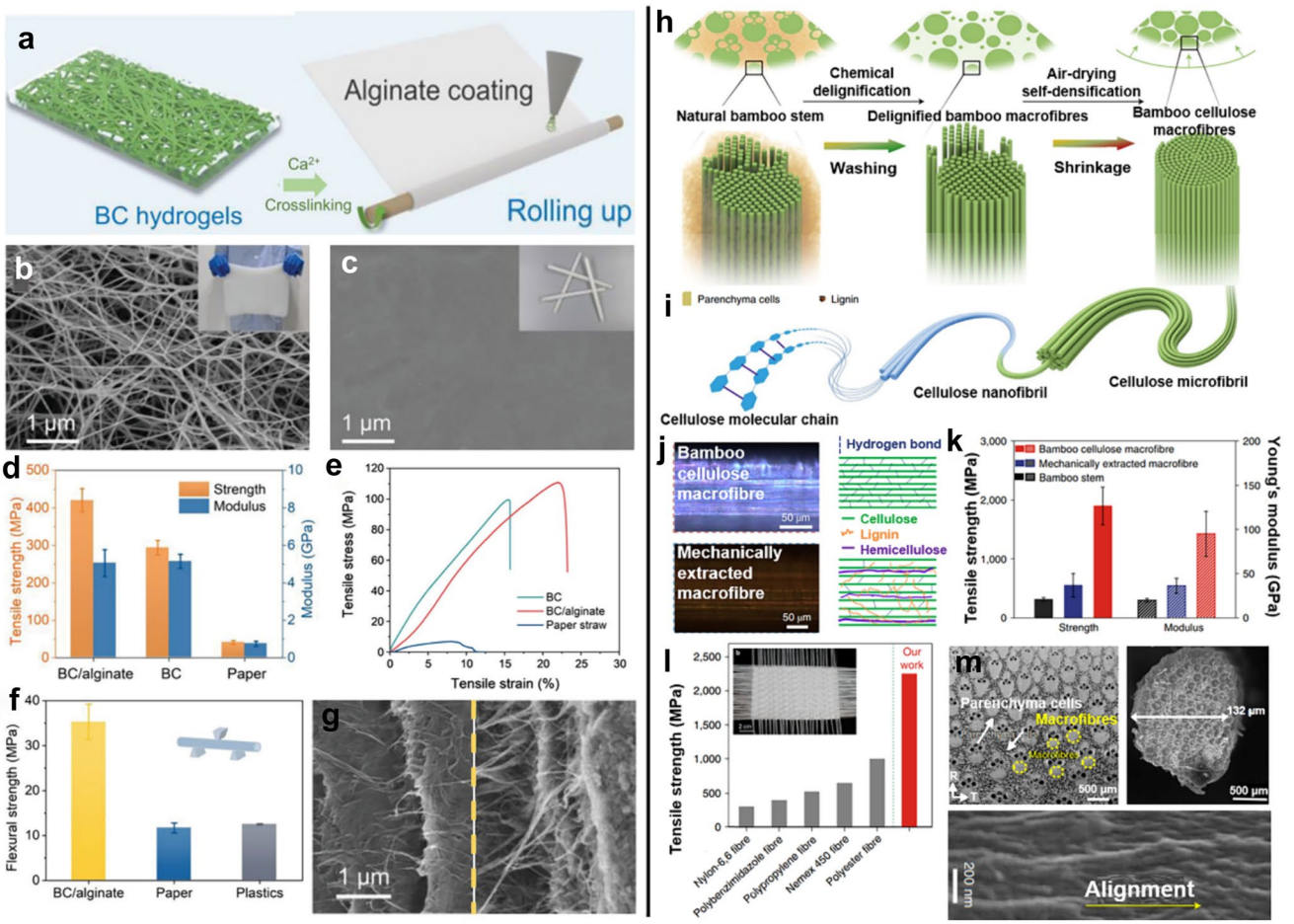

Fig. 3 **a** Preparation process of BC straw, **b**, **c** the SEM image of the BC aerogel and BC/alginate film, **d** tensile strength and elastic modulus of different straw materials, **e** wet stress–strain curves of different straws, **f** three-point bending strength of different straws, and **g** the SEM images of BC (left) and BC/SA (right) fracture cross-sections; Reproduced with permission from ref. [61], Copyright 2021, Wiley. **h** Preparation process of bamboo cellulose, **i** the structural composition of bamboo cellulose, **j** polarization microscope images and corresponding structural diagrams of chemically treated bamboo fibers (upper) and mechanically treated bamboo fibers (lower), **k** tensile strength and elastic modulus of different fibers, **l** comparison of tensile strength between bamboo cellulose large fibers and synthetic fibers with a photograph of bamboo fiber woven twill fabrics inset, and **m** the top–down SEM image of natural bamboo stems (upper left) and single bamboo fibers (upper right). The side views SEM image of microfibers arranged on the surface of bamboo fibers (lower); Reproduced with permission from ref. [64], Copyright 2021, Springer Nature

strategy, including chemical delignification and air drying, to extract high-performance cellulosic long fibers from natural bamboo stems in large quantities (Fig. 3h) [64]. First, crude bamboo cellulose fibers are separated from natural bamboo stems, and then a long cellulose fiber structure that contracts and densifies is formed through the capillary force of water evaporation (Fig. 3i). Chemical separation treatment uniformly removes amorphous hemicellulose and lignin, allowing bamboo fibers to align orderly through hydrogen bonds and exhibit vivid birefringence under a polarized light microscope. Nevertheless, some impurities persist even after mechanical extraction treatment, resulting in dim imaging (Fig. 3j). Compared with natural bamboo wood, chemically treated long fibers show a stronger average tensile strength of about (1.90 ± 0.32) GPa and a higher Young's modulus of about (91.3 ± 29.7) GPa, which is 7.2 and 6.2 times higher than that of the natural bamboo material, respectively (Fig. 3k). Furthermore, the tensile strength of the obtained sample is two times than those polymers-based synthetic fibers, such as nylon 66 fiber, polybenzimidazole fiber, polypropylene fiber, aromatic polyamide fiber, polyester, etc. (Fig. 3l). The framework of the natural bamboo core is an irregular structure composed of solid coarse fibers and hollow thin-walled cells. The chemical treatment effectively removes impurities while preserving long fibers, facilitating the exposure of hydrophilic hydroxy groups on the fiber surface and enhancing water absorption within the fibers. Subsequent air-drying evaporates the water between the fibers, causing the collapse of hydrogen bonding and capillary forces within the cellulose nanofibers, thereby

completing the process of fiber densification (Fig. 3m). The long fibers in the prepared bamboo fibers maintain a vertically arranged structure without evident detachment or leakage on the surface, indicating their exceptional mechanical properties. Substituting polymers and carbon fibers in structural composite materials with bamboo fiber holds promise for advancing sustainable development across various applications, including automobiles, aviation, and construction.

Single-component BC and bamboo fibers possess a relatively high degree of polymerization, resulting in higher ultimate tensile strength and improved tenacity. This production process, devoid of complex treatments, enables BC and bamboo fibers to maintain high crystallinity and strong inter- and intra-molecular hydrogen-bonding forces, thereby conferring excellent stiffness. Indeed, altering crucial parameters, such as strain, incubation time, and humidity during the generation process of these high-strength cellulose fibers can significantly influence their mechanical properties [65, 66], so future research on high-strength cellulose should incorporate highly standardized experimental methodologies from bioengineering theory.

3.2 Antibacterial Property

Similar to collagen, cellulose can also be effectively used as skin tissue adjuvant and wound care material [67], and due to the lack of antibacterial performances, it is necessary to endow it with antibacterial performances under physical/chemical modification [68]. Xie et al. successfully modified BC and cross-linked it with chitosan (CS) through carboxymethylation and selective oxidation techniques, resulting in the formation of dialdehyde carboxymethyl BC/CS (S-DCBC/CS) with antibacterial performances and promotion for wound healing [69]. Due to the micro-acidity of carboxylic acid, the carboxylic group can also enhance the positive charge of the amino group, thus preventing bacteria from absorbing trace elements and inhibiting bacterial reproduction (Fig. 4a). The cross-linking and permeation of chitosan led to an increase in the pore size of DCBC, while S-DCBC retained its 3D porous structure (Fig. 4b). Both CS and S-DCBC/CS showed excellent antibacterial activity against both *Escherichia coli* (*E. coli*) and *Staphylococcus aureus* (*S. aureus*), and the antibacterial rate was higher than 90%, and the inhibitory rate of S-DCBC/CS was higher than CS (Fig. 4c, d). The higher number of bacteria in S-DCBC/CS compared to CS can be attributed to the 3D nanonetwork structure of the composite material and the high-water content, which facilitate the adhesion and survival of bacteria (Fig. 4e). This phenomenon is referred to as "active" antibacterial action. The directional adhesive antibacterial effect of S-DCBC/CS gel formed by self-cross-linking is comparable to that of commercial antibacterial dressing.

In addition to the above "active" antibacterial action, there are also cellulose-based films with antibacterial activity which can be triggered under specific conditions. Liu et al. used TPEPy-modified glucose (Glc) as a carbon source to cultivate BC-based materials with photosensitivity and antibacterial properties (TPEPy-Glc-BC) [70]. As bacteria approach the surface of BC, the grafted photosensitizer generates reactive oxygen species (ROS) under light exposure. ROS have the capability to disrupt biomolecules, leading to deformation and collapse of the bacterial community, thereby inflicting damage on the bacteria. This process demonstrates the intrinsic biological killing effect (Fig. 4f). As the TPEPy-Glc-BC concentration increases, the bacterial community decreases more significantly, and the photosensitive TPEPy-Glc-BC also substantially strengthens its antibacterial capacity after light exposure (Fig. 4g). At the same time, cells were stained with propidium iodide (PI) and SYTO-9 to distinguish between living and dead cells in the same region. SYTO-9 can make cells appear green through the living cell film, while PI can only enter bacteria with damaged cell films. Exposure to light causes an increase in the concentration of TPEPy-Glc-BC, resulting in a significant rise in the proportion of red fluorescence and a noticeable weakening of green fluorescence. This phenomenon signifies that sufficient ROS are produced by TPEPy-Glc-BC to destroy the survival of *E. coli* and *S. aureus* (Fig. 4h). Under conditions with or without light, there was no significant change in the morphology of *E. coli* and *S. aureus* on the BC film (Fig. 4i). After being exposed to light, *E. coli* and *S. aureus* on the TPEPy-Glc-BC film began to collapse and deform, which were originally intact and smooth. All the data above indicate that TPEPy-Glc-BC attacks and eliminates common pathogenic bacteria under light stimulation, which is the application of "passive" antibacterial. Antimicrobial agents typically require direct contact with bacteria to exert their antimicrobial effect. Hence, these agents are usually located on the surface of antimicrobial cellulose composites [71, 72]. Therefore, antimicrobial cellulose composites need to be protected from surface contamination adhesion. The antimicrobial or bactericidal properties of cellulose composites in wet environments or underwater scenarios should also be considered.

3.3 Gas Regulation and Detection

Packaging provides the necessary survival conditions for the product by adjusting the gas and water content in the packaging environment and prevents structural deterioration by inhibiting the growth of microorganisms. In addition to extending the shelf life of the product, packaging should

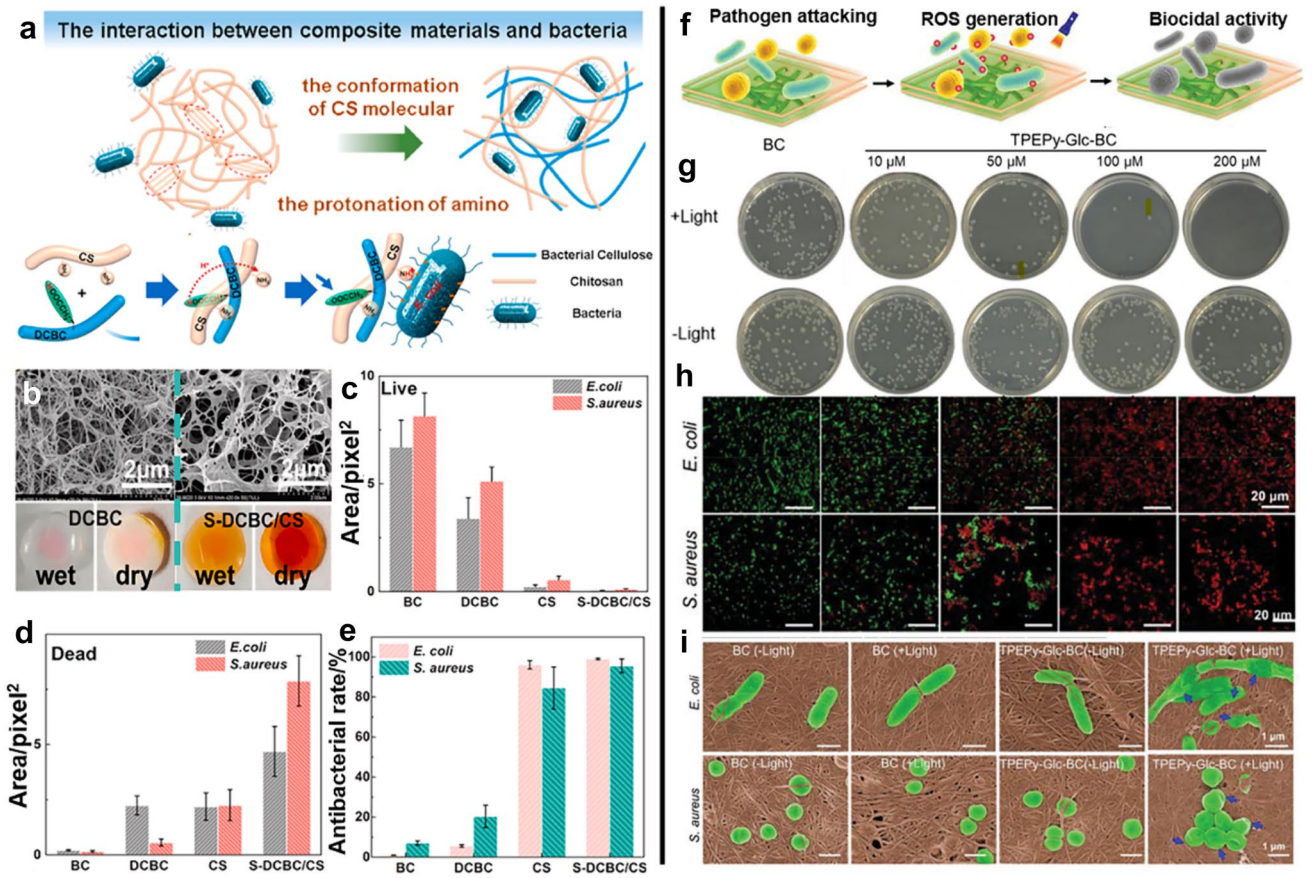

Fig. 4 **a** Schematic diagram of S-DCBC/CS by antimicrobial effects of composite, **b** SEM images of DCBC and S-DCBC/CS, as well as corresponding digital images under dry and wet conditions, **c**, **d** statistics of the area of live and dead bacteria on surfaces with different samples, **e** inhibition rate of the different samples; Reproduced with permission from ref. [69], Copyright 2022, Elsevier. **f** Schematic demonstration of the bactericidal functions of TPEPy-Glc-BC, **g** LB agar plates of BC and different concentrations of TPEPy-Glc-BC under light and darkness, **h** staining of viable and dead cells of *E. coli* and *S. aureus* in BC and TPEPy-Glc-BC of different concentrations under light conditions, **i** SEM images of *E. coli* and *S. aureus* on BC and TPEPy-Glc-BC under light and dark conditions; Reproduced with permission from ref. [70], Copyright 2022, Wiley

also possess the qualities of biocompatible, biodegradable, and safe for human use. Therefore, cellulose-based packaging has become the research focus of modified atmosphere packaging. Jung et al. developed a gas barrier coating comprised of CNCs/curcumin/polyprotein (CNC/Cur/PPr) for fruit preservation via a dip coating [73]. Although the film appears yellow, it still retains a certain level of light transmittance, facilitating the observation of food spoilage even when applied to the surface of fruits (Fig. 5a). The fruits coated by the sample can maintain their appearance for more than 11 days both in the appearance and interior, and no enzymatic browning and decay were observed (Fig. 5b). Furthermore, strawberries protected by CNCs/Cur/PPr retained more than 65% of their original weight after 1 week (Fig. 5c). The weight loss of the coated fruits was significantly lower than that of the uncoated fruits. The water vapor transmission rate (WVTR) of the coating is about 15 g·mm/(m^2·day), which is lower than other common biopolymers used for packaging, including chitosan, polylactic acid (PLA), pectin, protein isolate, and starch-based composites (Fig. 5d). The oxygen permeability (OP) of the coating measures is about 20 cm^3·μm/(m^2·day·kPa), which is also lower than commercial packaging materials (Fig. 5e). The exceptional water vapor transmission rate (WVTR) and oxygen permeability (OP) properties of the film can be attributed to the high crystallinity and uniformity of the incorporated CNCs, facilitating the formation of a denser and more uniform coating [74]. Reprocessing natural edible materials sourced from waste can extend food preservation, providing an alternative to costly and time-consuming wax-based packaging, as well as avoiding the use of non-degradable plastic packaging.

When food packaging relies solely on limiting water vapor transmission rate (WVTR) and oxygen permeability (OP), users can only assess food spoilage visually. However, by designing packaging materials with self-powered

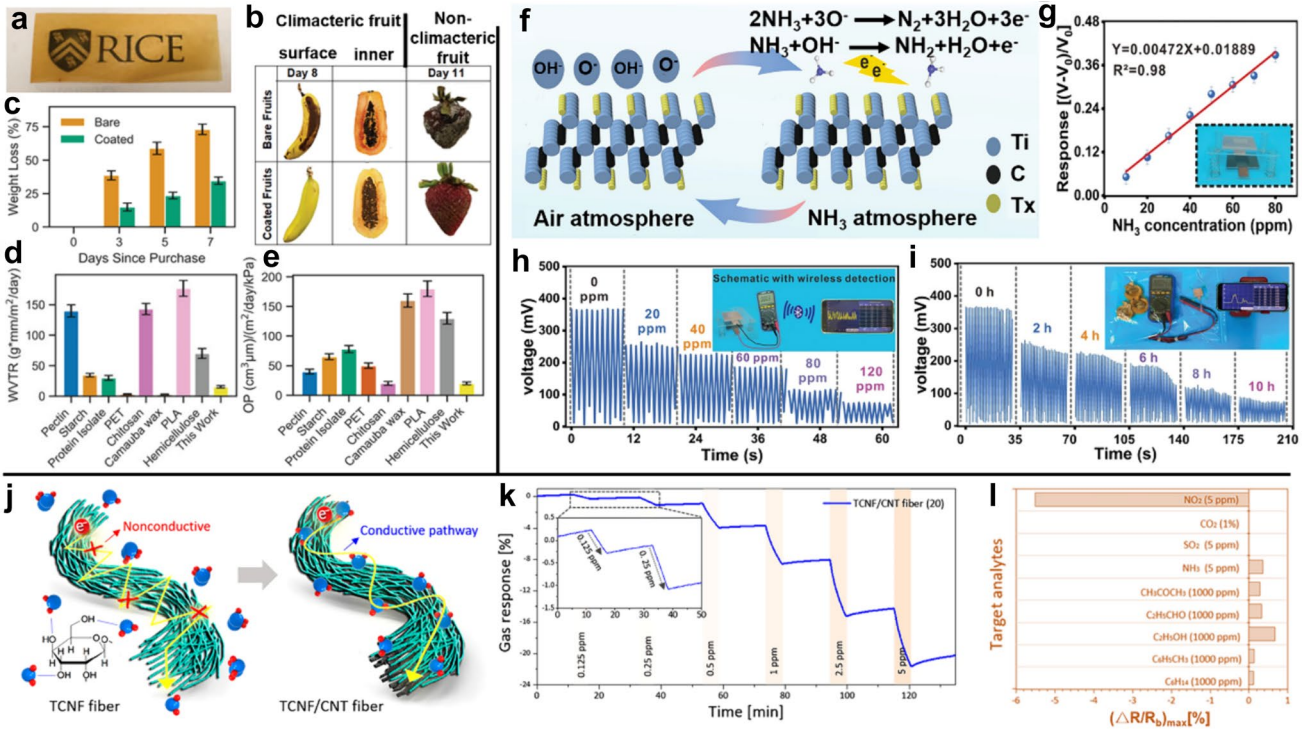

Fig. 5 **a** Photograph of CNCs/Cur/PP, **b** comparison of Time-lapse photographs of bare and coated climacteric fruits, internal slices of fruits, and non-climacteric fruits, **c** comparison of weight loss of bare and coated strawberry after several days, **d** comparison of WVTR between nanocomposite films and other polymer coatings, and **e** comparison of OP between nanocomposite films and other polymer coatings; reproduced with permission from ref. [73], Copyright 2020, Wiley. **f** Schematic diagram of NH_3 sensing mechanism, **g** response fitting curves of TENG at different NH_3 concentrations, **h** wireless sensing voltage signals from exposure to different concentrations of NH_3, and **i** wireless sensing voltage signals at different times of food spoilage; reproduced with permission from ref. [75], Copyright 2022, Wiley. **j** Sensing mechanism of the TCNF/CNT fiber, **k** response of resistance changes of TCNF/CNT (20 wt%) at Different NO_2 concentrations, and **l** maximum value of resistance change rate of TCNF/CNT (20 wt%) for different tested objects; reproduced with permission from ref. [76], Copyright 2019, American Chemical Society

capabilities, users can engage in real-time monitoring through wireless sensors. Therefore, developing gas sensors for rapid identification and accurate monitoring of target gases emerges as a crucial task in scientific research. Zhang et al. constructed a gas-sensitive cellulose triboelectric ($Ti_3C_2T_x$-CNF) through intermittent suction filtration that can be used for NH_3 sensing with high adsorption [75]. When the film is exposed to NH_3, the gas molecules are adsorbed on the active sites on the $Ti_3C_2T_x$ sheet through the dispersion force between ammonia molecules and the functional groups or defects (Fig. 5f). When NH_3 enters the electrostatic field, it is adsorbed on the negative electrode frictional material, while the negative electrode collects electrons to complete gas sensing detection. The sensitivity of the electrode material is defined by the linear fitting of the voltage change graph, with values of 0.98, indicating that the TENG exhibits good linearity as an NH_3 sensor (Fig. 5g). The gas-sensitive CNF sensor demonstrates the potential for wireless real-time sensing applications and exhibits long-term stability when monitoring the concentration of ammonia in spoiled food over varying durations (Fig. 5h, i).

Cellulose-based materials can also serve as gas detectors to detect gas pollutants in the environment. Cho et al. reported fiber sensing materials (TCNF/CNT) with excellent mechanical and sensing properties through the wet spinning process [76]. The terminal hydroxy group that existed in TCNF is alkaline and nucleophilic, acidic gases such as NO_2 could be automatically adsorbed on the surface of TCNF fibers [77]. Due to the insulating property of TCNF, even if a large amount of NO_2 is adsorbed on the fiber, the change of conductivity cannot be observed [78]. In TCNF/CNT fibers, CNT can form a conductive path for TCNF fiber bundles (Fig. 5j). TCNF/CNT fibers change conductivity during the adsorption of NO_2, thereby completing the detection of NO_2. The combination of acidic NO_2 with hydroxy groups on TCNF leads to the accumulation of charges and affects the conductivity of CNT in the material, thereby reducing the resistance of the sample. When the concentrations of NO_2 were at 0.125 and 0.25 ppm, a significant difference in the response rate of TCNF/CNT fiber was observed, showing a sensitivity of TCNF/CNT fiber to NO_2 of 1 part per billion (Fig. 5k). Compared with other gas molecules such as CO_2,

SO_2, etc., TCNF/CNT (20 wt%) exhibits a significant change in the resistance value when exposed to NO_2 (Fig. 5l), which can be attributed to the higher acidity of NO_2 compared to CO_2 and SO_2, making it easier to bind with hydroxy groups on TCNF. Moreover, among the tested volatile organic compounds, ethanol exhibits a significant change in resistance compared to other organic volatile molecules, suggesting the potential for diverse applications of TCNF/CNT fiber. TCNF/CNT fiber can be effectively employed in wearable sensing materials to achieve highly sensitive selectivity to specific gases.

Food packaging acts as an airtight seal to protect food from the risk of contaminating agents, such as oxygen, microorganisms, water vapor, and odors, thereby extending the shelf life of the food [79]. Higher crystallinity cellulose provides a compact structure and density, thus impeding free space for gas molecules to migrate. However, cellulose contains abundant hydroxy groups on its surface, which have a tendency to absorb water and may facilitate the growth of bacterial strains in humid environments [80]. Hence, hydrophobicity needs to be taken into account for the application of cellulose materials in food packaging. Additionally, the incorporation of antimicrobial agents and pH indicators should also consider their dispersion within the cellulose matrix.

3.4 Hydrophobic Property

The hydrophilic and non-waterproof nature of intrinsic cellulose paper significantly restricts its potential for "cellulose paper-based plastic substitution". Undoubtedly, there is an urgent need for the superhydrophobic modification of cellulosic paper-based materials and the expansion of their high-value-added applications [81, 82]. Wang et al. developed a novel hydrophilic/superhydrophobic patterned surface (SHS-HI) through the self-assembly of CNC and wax microspheres to enhance its water capture and transport performance [83]. In the ultra-hydrophobic Cassie-Baxter state, water droplets can easily roll off the surface and can be removed quickly due to the air cushion present on the rough surface (Fig. 6a). When water droplets come into contact with the surface downwards, they gradually deform (Fig. 6b). When water droplets completely detach from the surface, their volume remains unchanged, indicating that the superhydrophobic/superoleophilic surface (SHS-HI) can adhere to water droplets but is not easily soaked by water. The surface adhesion of SHS-HI is 27.6 μN, exhibiting a relatively uniform surface structure (Fig. 6c). As the density of CNC increases, the difference between the advancing contact angle (ACA) and receding contact angle (RCA) increases. This indicates that an increase in the proportion of CNC makes it easier for water droplets to wet the surface of SHS-HI (Fig. 6d). When the contact line of the droplet surface begins to retract from the adjacent column, the droplet needs to overcome the huge energy barrier of the surface with high-density hydrophilic region [84]. The overall surface free energy of SHS-HI surface is 38.0 mJ/m^2, which is much higher than the pure wax surface of 25.4 mJ/m^2 (Fig. 6e). This is due to the strong interaction between the surface and small water droplets through hydrogen bonding during the liquid collection process, which increases their surface free energy and minimizes the kinetic energy during the water droplet nucleation process, thereby improving the water collection ability of the SHS-HI surface [85]. The dynamic contact angle and static contact angle of the SHS-HI surface before and after dust abrasion show no significant difference, indicating that the hydrophobic surface can maintain its mechanical robustness under adverse conditions (Fig. 6f). The structural design of superhydrophobic SHS-HI surfaces under foggy conditions can offer an effective strategy for water collection systems.

Fluorocarbon compounds can pose significant harm to the environment, prompting a shift toward research on environmentally friendly fluorine-free hydrophobic compounds. Zhao et al. developed a fluorine-free, efficient, and biodegradable waterproof and breathable film by heat treating cellulose acetate (CA) impregnated with hyperbranched polymers (Fig. 6g) [86]. The interconnected network and high porosity provide enough channels for water transport, making the film permeable. The waterproof ability of TCA comes from the hydrophobic inner surface and clear geometric pores (Fig. 6h). When the dyed water droplets are placed on the surface of the CA film, they quickly wet and dye the surface in a very short time, while the water on the TCA film moves rapidly, indicating that TCA has excellent liquid repellency (Fig. 6i). The WCA of TCA showed no significant changes after undergoing sandpaper cyclic wear and long-term ultrasonic washing, indicating the stability and durability of TCA (Fig. 6j, k). The design of fluorine-free, hydrophobic, and biodegradable TCA reduces the impact on the natural environment, while its efficient hydrophobic performance in complex environments also meets daily protection and use.

The expansion of superhydrophobic modification of sustainable cellulose paper for functional devices is urgently needed. The stability of superhydrophobic cellulose materials and the simplification of the preparation process remain hot topics in current research [87, 88]. Meanwhile, green biopolymers can be used in the preparation process to avoid the use of toxic reagents that are harmful to the environment and the human body.

3.5 Other Performance

In addition to the above characteristics, cellulose has gradually been developed with more characteristics due to its

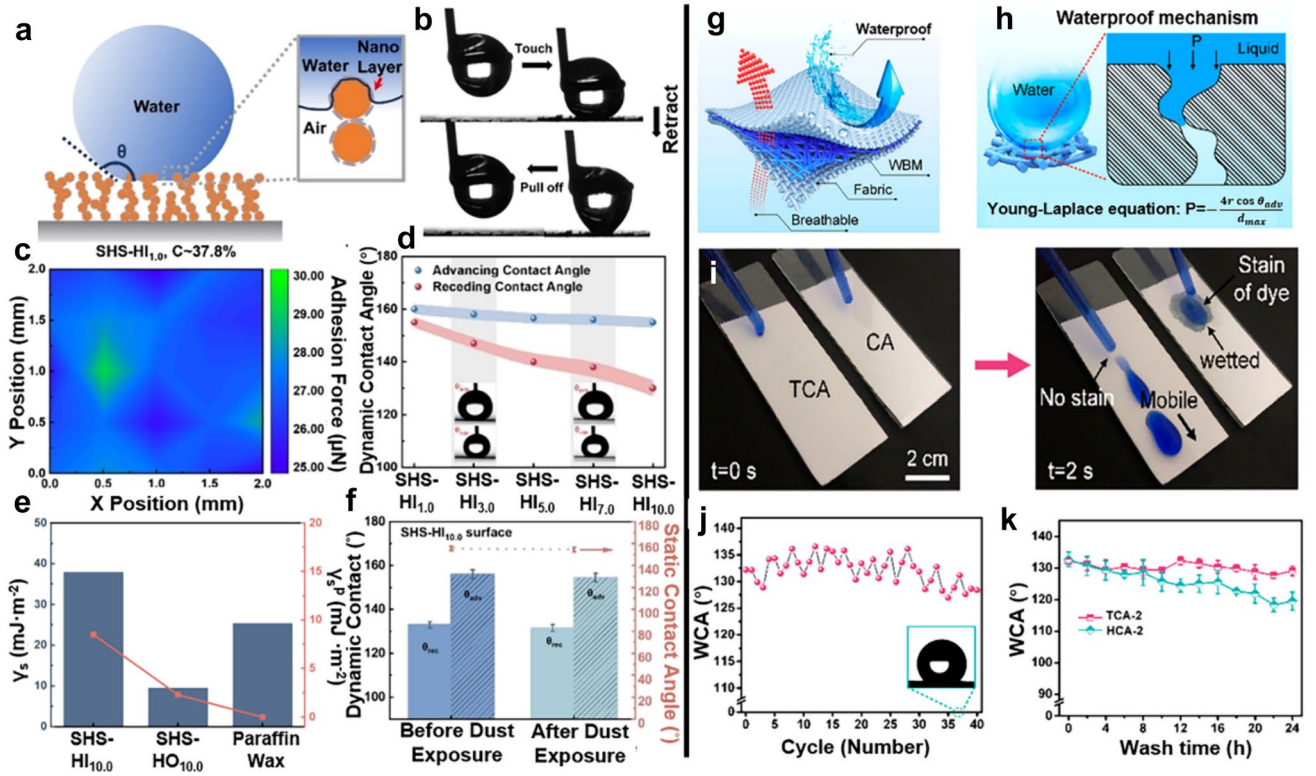

Fig. 6 **a** Schematic diagram of infiltration on the surface of superhydrophobic SHS-HI, **b** tensile adhesion testing procedure on SHS-$HI_{1.0}$, **c** the surface adhesion mapping of SHS-$HI_{1.0}$, **d** the ACA and RCA of different surfaces, **e** surface free energy and dipolar–dipolar interaction force of different surfaces, and **f** changes in the dynamic contact angles and static contact angles before and after dust exposure; reproduced with permission from ref. [83], Copyright 2022, Wiley. **g** Schematic diagram of waterproof breathable properties of TCA, **h** waterproof mechanism based on the Young–Laplace equation, **i** comparison of wetting properties of dyed water on the sloping surface of CA and TCA films, and **j** plot of WCA after each abrasion cycle. The inset is the WCA after the 36th cycle abrasion, **k** the variation of WCA with washing time; reproduced with permission from ref. [86], Copyright 2020, American Chemical Society

excellent properties. As a potential thermal management material for energy-saving applications used in buildings, cellulose foam has attracted extensive attention [89, 90]. Hou et al. prepared plant cellulose-based foam (PCF) with pulp fiber, CNF, and borate, in which borate is used as both flame retardant and cross-linking agent to build a solid porous and layered structure with the fiber, while CNF can be used as a stabilizer to ensure good foaming ability and improve the stability of the foam [91]. The surface temperature of various products did not change significantly within 30 min, and the overall temperature of the sample decreased from bottom to top (Fig. 7a, b). PCF serves as an excellent thermal insulation material, filled with numerous bubbles inside, which reduces the rate of temperature transfer and effectively isolates heat in the perpendicular direction. The enhanced intensity of the B–O–C bending vibration peak at 1430 cm^{-1} indicates the cross-linking of borate ester and the hydroxy groups of cellulose. Moreover, it indicates the formation of a stable covalent bond between borate and cellulose (Fig. 7c).

Apart from efficient thermal insulation performance, cellulose-based 3D materials can also achieve rapid water transport capacity through hydrophilic hydroxy functional groups, which can be used in seawater desalination and wastewater treatment [89, 92]. The interface solar steam power generation (ISSG) provides a sustainable means to overcome the emergencies of freshwater shortage [93, 94]. Lin et al. reported a double-layer hydrogel evaporator based on lignocellulose hydrogel (LCG) and lignin-derived carbon (LC), which served as the matrix and photothermal materials, respectively, for efficient solar desalination [95]. Four main ions (Na^+, Mg^{2+}, $K^{+,}$ and Ca^{2+}) were used to evaluate the desalination performance of LC@LCG (Fig. 7d). The concentrations of various ions in the original seawater are initially high, but they decrease significantly after treatment with LC@LCG, meeting the drinking water standards set by the World Health Organization (Fig. 7e) [96]. Due to the hydrophilicity of the film and the abundance of pores, these pores can rapidly pump water up and continuously dilute the salt water on the top evaporation surface [97]. LC@LCG

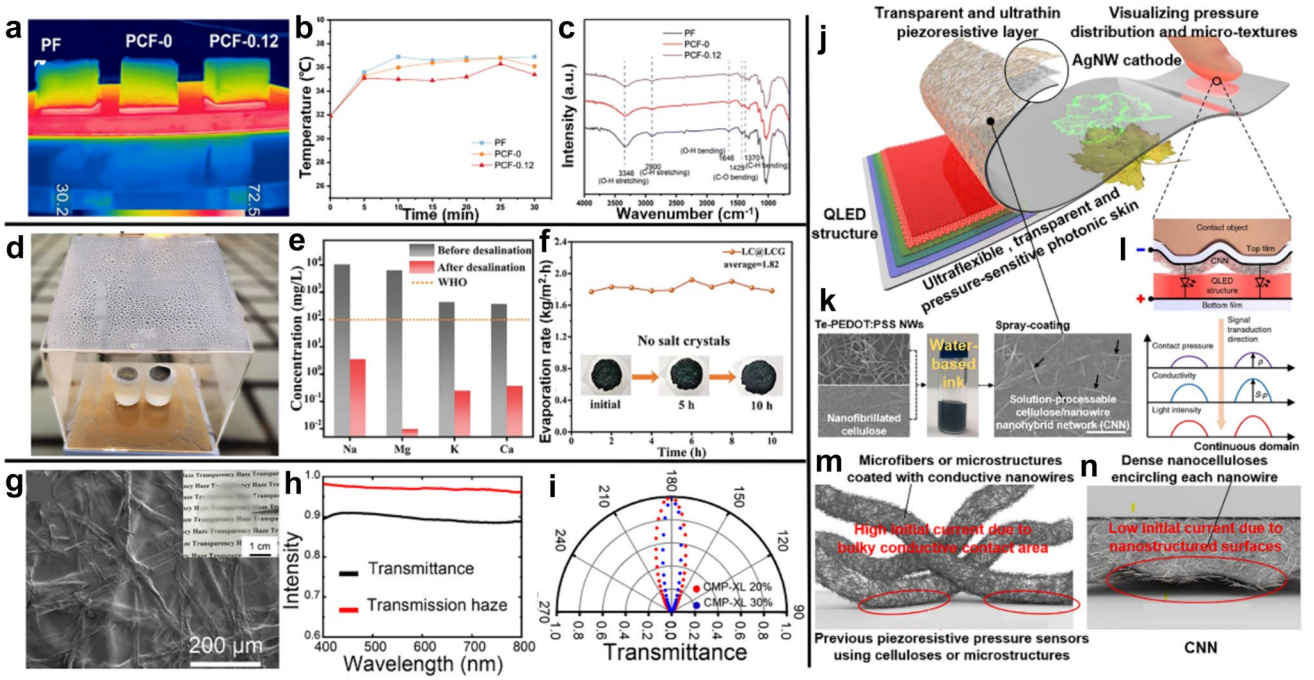

Fig. 7 **a** IR images of the side of different foams on a heating plate at 70 °C, **b** the surface temperature curves of different foams, **c** FTIR spectra image of different foams; reproduced with permission from ref. [91], Copyright 2023, Royal Society of Chemistry. **d** LC@LCG's outdoor desalination plant, **e** comparison of ion concentration before and after desalination using LC@LCG, and **f** long-term stability evaluation of LC@LCG in 3.5 wt% saline water and corresponding actual digital photos; reproduced with permission from ref. [95], Copyright 2022, Wiley. **g** SEM image and digital image of the surface of a composite film with 20% CMP-XL, **h** transmittance and haze spectra of 20% CMP-XL film, and **i** light intensity angle distribution diagram of 20% CMP-XL and 30% CMP-XL; reproduced with permission from ref. [98], Copyright 2022, American Chemical Society. **j** Concept diagram of a device structure for e-skin, **k** CNN's manufacturing plan and form, **l** schematic of super-resolution and high contrast pressure imaging, **m** the working mechanism of cellulose pressure sensors in the past, and **n** the working mechanism of CNN micro-structure pressure sensor; reproduced with permission from ref. [101], Copyright 2020, Springer Nature

maintains a stable average evaporation rate of 1.82 kg/(m^2·h) with high efficiency and exhibits satisfactory salt resistance within 10 h without the formation of crystalline salts on the surface (Fig. 7f). Porous lignocellulose-based hydrogels hold promise for applications in water treatment due to their outstanding solar-driven evaporation rate, resistance to salt, and desalination performance.

High refractive index inorganic nanoparticles are frequently incorporated into optical management electronic components. However, their accumulation in the environment has become a growing concern, contributing to the prominent issue of electronic waste. Additionally, the fiber network structure of cellulose itself can contribute to light management, serving as degradable light-scattering enhancers and potentially replacing traditional inorganic nanoparticles. Yang et al. prepared cellulose microparticles (CMP) of different sizes, including small-width microparticles (CMP-S), medium-width (CMP-M), large-width (CMP-L), and larger width microparticles (CMP-XL) by adjusting sulfuric acid concentration, reaction time, and temperature [98]. CMP and CMC are added into films that can be spatially arranged in disordered networks to generate high scattering and optical haze materials, as well as optimize scattering performance at a single scattering level. CMP-XL is distributed as a cutting element within the CMC matrix, thereby increasing the stacking density of cellulose paper (Fig. 7g). The top part of the cellulose paper appears blurry when it is away from the background board, while the bottom part exhibits high transparency when it is attached to the background board. The CMC is embedded in the gaps of CMP-XL to ensure the transparency of the fiber paper, while an increase in micron-level cellulose content will improve the internal unevenness of the fiber paper, thereby increasing the haze. Cellulose paper maintains a transmittance of about 90% within the visible light wavelength range and exhibits a high haze of over 92% (Fig. 7h). The transmission of the transmitted beam through the CMP-XL film at a non-normal angle suggests that the CMP-XL film restricts the beam after a certain angle deviation, providing further confirmation of the high haze performance of the CMP-XL film (Fig. 7i). Cellulose-based optical materials with biocompatibility and sustainable development can be used in solar electronic devices, ink pigments, and anti-glare materials.

Sensing devices have garnered significant attention across various fields, particularly in medical prostheses and intelligent human–machine interactive systems. Currently, sensors characterized by fast response speed, high sensitivity, and sophisticated data acquisition capabilities are crucial for the development of intelligent human–machine systems [99, 100]. Lee et al. reported an ultra-flexible and transparent pressure-sensitive electroluminescent skin, which can automatically display high-resolution images of real-time pressure distribution (Fig. 7j) [101]. The device consists of a transparent pressure-sensing film and an electroluminescent film. The pressure-sensing film comprises a network of cellulose nanowires (CNN) and a layer of transparent Ag nanowires (Ag NWs), which serves as the common cathode. The electroluminescent film serves as the electron transport layer (ETL) of a quantum dot light-emitting diode (QLED). Previously, cellulose pressure sensors were coated with conductive nanowires (Fig. 7m) [102–105]. To achieve ultra-thin and high sensitivity designs, dense CNN nanofibers are wrapped around each tellurium poly(3,4-ethylened ioxythiophene):poly(styrenesulfonate) (Te-PEDOT:PSS) nanowire, the mixed ink is solvable to ensure the uniformity of the mixture (Fig. 7k). The low specific surface area of the exposed nanowires indicates a small initial conductive contact area, leading to an initially low current and high sensitivity. The wide working range and high linearity of the cellulose nanowire network (CNN) can be attributed to its nanostructured surface (Fig. 7n). When the top and bottom films of electronic skin (e-skin) are consistent with the contact object, the CNN of the top film contacts the ETL and forms a conductivity distribution between the cathode and ETL, which is linearly related to the pressure distribution (Fig. 7l). Space signals are transmitted as analog signals from pressure to light intensity, and e-skin can achieve visualization of pressure distribution without the need for pixel structures [106].

4 Applications of Cellulose-Based Materials

Cellulose, which has a wide range of sources, biodegradability, and high-strength mechanical properties, can be widely used as a substitute for plastic materials such as disposable straws, tableware, and cling films. Simultaneously, cellulose with excellent hydrophilicity, water retention, and non-toxic properties can also be used in medical supplies such as disposable wound dressings and electronic monitoring. Multi-functional cellulose is not only suitable for large-scale production of products but also possesses the potential to develop electrochemical energy storage materials. The adjustable pore distribution and functional surface of cellulose can effectively inhibit the growth of dendrites when it is employed as a battery separator. The high porosity and specific surface area facilitated by a large amount of entangled cellulose can enhance material transport in electrochemical devices.

4.1 Food Packaging and Disposable Tableware

So far, plastics derived from petroleum-based polymers have been developed for more than 100 years. The plastics are extruded into any shape by hot melting, including building materials, disposable food preservation film, and tableware. Due to their chemical stability and biological inertness, the plastics could remain in the environment for hundreds of years, and thus threaten the environment and human health. Despite the rapid development of cellulose-based biodegradable materials, paper-based materials encounter challenges related to the necessity for binders and waterproofing additives [107]. Wang et al. proposed an all-natural cellulose-based straw based on the composite of cellulose nanofiber and cellulose microfiber without additional adhesive [108]. Large-scale acquisition of cellulose nanofibers and cellulose microfibers is typically obtained from bagasse and wood. These fibers are then mixed and filtered to form a wet film. Subsequently, the wet hybrid cellulose film is rolled into the shape of a straw. After drying, the edges of the film can be sealed through a large amount of hydrogen bonds (Fig. 8a). After degrading in the natural environment for 120 days, the cellulose nanofiber-based straw had completely disappeared, and the cellulose hybrid straw was decomposed into fragments while no significant change was found in the plastic straw. Therefore, the cellulose hybrid straw can be used as a highly natural degradable material to replace disposable plastic straws (Fig. 8b). The flexural strength and tensile strength of the cell hybrid straw is 6.9 ± 0.8 MPa and 70 MPa, respectively, which is superior to other types of straws (Fig. 8c, d). The interaction forces between cellulose in different states were simulated through classical full molecular dynamics. During the stretching process, the cellulose chains do not break; instead, relative slipping occurs between cellulose fibers. In the cellulose hybrid strand, cellulose nanofibers are arranged around cellulose microfibers in a hexagonal configuration pattern, illustrating the relative sliding of adjacent cellulose fibers under stress. This configuration confirms the excellent mechanical properties of the composite cellulose (Fig. 8e). Cellulose has garnered widespread attention due to its unparalleled advantages, such as low cost, full degradability, and excellent mechanical properties. These attributes provide strong competitiveness as a substitute for plastic straws.

Paper-based food materials are promising substitutes. However, even when they are coated with non-degradable plastic coatings, they can still show swelling caused by hydration [109]. Liu et al. constructed a hydrophobic EC film through the addition of SiO_2 [110]. Sun et al.

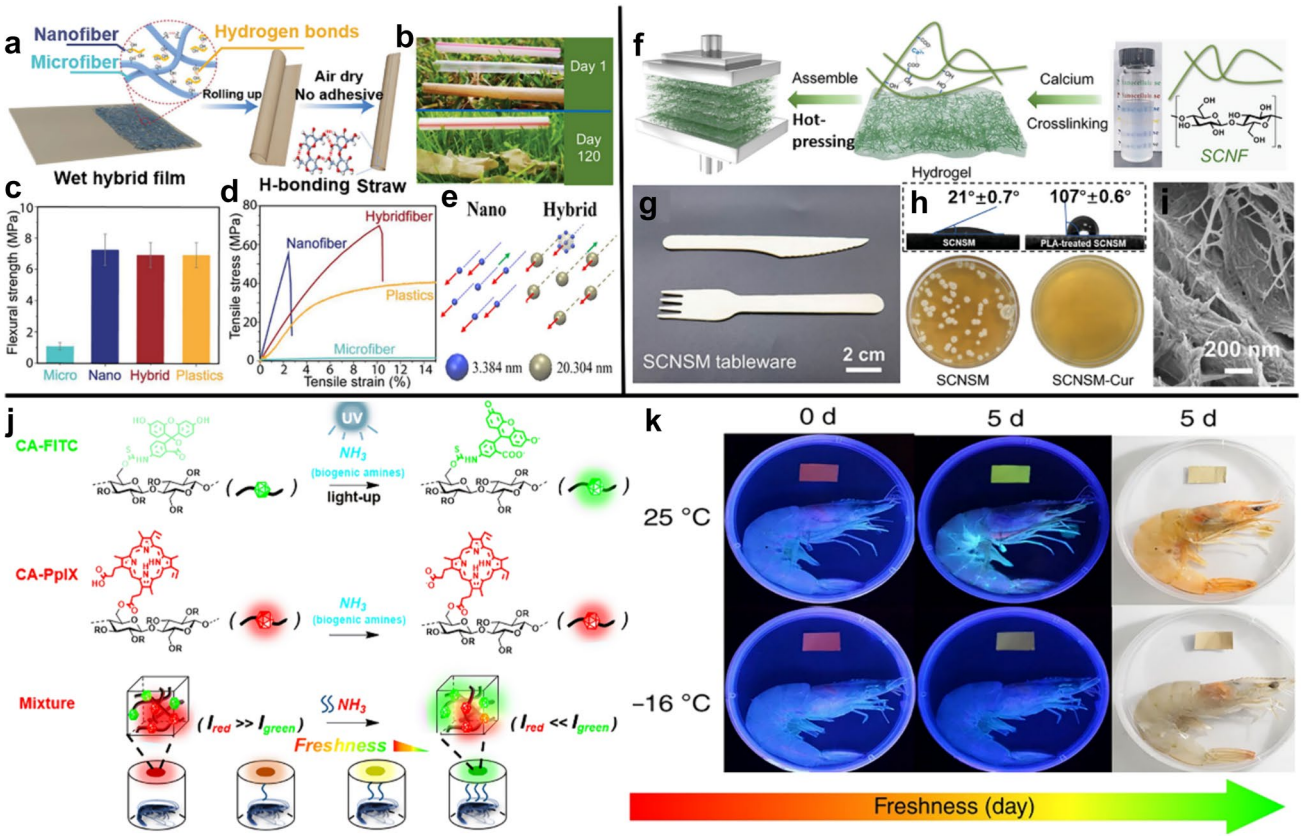

Fig. 8 **a** Manufacturing schematic diagram of cellulose hybrid straws, **b** degradation tests on various straws, **c** comparison of flexural strength of various straws, **d** the tensile stress–strain curves of various films, and **e** schematic diagram of simulation models for cellulose nanofibers and hybrid fibers. Colored circles represent CG beads with different sizes; reproduced with permission from ref. [108], Copyright 2020, Wiley. **f** The preparation process of SCNSM, **g** Photograph of SCNSM disposable tableware, **h** comparison of WCA between SCNSM and PLA-treated SCNSM (upper). Comparison of antibacterial tests between SCNSM tableware and SCNSM-Cur tableware (lower), and **i** SEM image of SCNSM sample; reproduced with permission from ref. [58], Copyright 2022, Wiley. **j** Design, synthesis, and mechanism of action of cellulose-based fluorescent materials responsive to ratio type amines, and **k** Intelligent tag ACRF for in-situ monitoring of shrimp freshness; reproduced with permission from ref. [34], Copyright 2019, Springer Nature

improved the hydrophobicity of cellulose paper and weakened the capillarity by covalently combining rosin-based modifiers with a cellulose fiber network [111]. While biocompatible natural hydrophobic materials can be expensive, they indeed improve the water resistance of cellulose films. Ki et al. reported a disposable biodegradable tableware with excellent mechanical and thermal properties, which is made of sargassum cellulose nanofiber (SCNF) [58]. After introducing Ca^{2+} into SCNF suspension, the coordination bonds and abundant hydrogen bonds between cellulose made the suspension form the hydrogel. The cellulose hydrogels, stacked layer by layer, are subjected to heat and pressure to remove most of the free water, thus preparing sargassum cellulosic-based structural materials (SCNSM) (Fig. 8f). SCNSM can be molded into different utensils to meet the practical application needs, such as knives and forks (Fig. 8g). Highly biocompatible polylactic acid (PLA) coating and Cur modification were made to endow the SCNSM tableware hydrophobicity and antibacterial properties. After the treatment of PLA, the WCA of SCNSM increased from 21° to 107°. Introducing Cur on a cellulose substrate, the number of bacteria in SCNSM-Cur tableware is much smaller than that of SCNSM tableware, demonstrating the excellent antibacterial effect of SCNSM-Cur tableware (Fig. 8h). Due to the certain disorder degree of fiber and the presence of nanopores, the cellulose film can be loaded on multiple substances with different weight (Fig. 8i) [112].

Food corruption is one of the most important problems for consumers and the food industry [113]. Rotten food can lead to significant economic losses and pose serious health risks. Real-time monitoring of various food quality indicators, such as pH changes, oxygen levels, temperature, etc., is an effective method for identifying food deterioration [114]. Jia et al. designed and prepared an amine-responsive cellulose-based radiometric fluorescent material (ACRF), which

can detect the freshness of seafood [34]. The obtained green light-emitting CA-fluorescein isothiocyanate (FITC) was mixed with red light-emitting CA-PpIX in a certain proportion to obtain a solid fluorescent material with adjustable fluorescence. After the film is exposed to ammonia, the protons of FITC are deprived, and the changes in molecular structure lead to the enhancement of green fluorescence. The fluorescent color change from red to orange, yellow or green, is easily discernible by any untrained observer (Fig. 8j) [115]. After 5 days of storage at 25 °C, the fluorescence color of ACRF changed to light green, while after 5 days of storage at −16 °C, the fluorescence color of ACRF changed to orange (Fig. 8k). The method for detection of the food freshness is simple, speedy, and accurate, making it significant for ensuring food safety and provides practical application for food enterprises.

The use of disposable tableware has brought convenience to people's lives. However, given the massive global consumption every year, it is imperative that we transition to biodegradable materials as an alternative to plastic disposable tableware. Based on existing research, it is known that disposable cellulose tableware not only has sufficient mechanical strength but also has a certain degree of water resistance. Most of the oil repellents in plant fiber tableware is currently available on the market are fluorine-containing. Therefore, in the development process of disposable cellulose tableware should be used to further improve its oleophobicity using environmentally friendly materials.

4.2 Medical Supplies

Faced with changes in society and the pursuit of a healthy lifestyle, people pay more attention to their health status, which further promotes the rapid development of medical equipment. Wearable devices have attracted people's attention in various fields, especially in healthcare and related products [116]. Diversified and available cellulose-based wearable devices can be compounded with additives for wider applications in the medical field [117–119].

Zhao et al. prepared a multi-functional intelligent fabric (M-fabric) via the combination of MXene and flexible cellulose fabrics and applied it to health care and biomedicine [120]. The MXene is deposited on the surface of cellulose fabric through the strong hydrogen bond, making it a composite fabric with excellent conductivity and joule heat function. The multi-functional flexible electronic M-fabric serves three major functions. MXene sheets are deposited on the surface of cellulose fabric without affecting the random overlap between fibers, thereby ensuring the permeability of the composite fabric. MXene combines with water molecules through functional groups such as –OH and –O, and as a result, the interlayer spacing between MXene sheets was changed, resulting in changes in the resistance of M-fabric. M-fabric monitors the health status of patients with respiratory illnesses through changes in moisture in the environment (Fig. 9a). The resistance response of MXene for dehydration/adsorption of water is utilized to monitor the resistance change caused by dehydration during the heating process, thereby indirectly providing feedback on the heating effect of joule heat. M-fabric can be applied as an external hot compress on various body parts to alleviate skin and muscle stiffness, enhance blood circulation, and alleviate pain. When the M-fabric is connected to the alarm circuit, it can also emit a high-temperature alarm, effectively preventing skin burns during the hyperthermia process (Fig. 9b). The third is to use the electrothermal effect of the M-fabric to eliminate the bacteria in the bacterially infected wound and enhance the effect of promoting wound repair (Fig. 9c). M-fabric showed the fastest wound healing and no wound inflammation when applied voltage due to the intrinsic performance of MXene for causing bacterial film rupture and inhibiting bacterial growth (Fig. 9d). Wounds treated with M-fabric under voltage did not show severe cell tissue necrosis, with few inflammatory cells and large amounts of collagen fibers produced. The results demonstrate that the heating effect of M-fabric effectively eliminates bacterial infection and promotes tissue regeneration and wound healing (Fig. 9e, f). The M-fabric, being safe and reliable, exhibits great potential as an integrated wearable electronic device for respiratory monitoring, intelligent hyperthermia, and wound healing.

Considering the outbreak of COVID-19 in recent years and the impact of particulate matter pollution, there is a growing demand for healthcare supplies especially wearable smart masks to prevent virus transmission and protect human health [121, 122]. However, the bulky traditional respiratory monitoring system limits its application in personal healthcare. Moreover, wearable electronic products still have many shortcomings in terms of power supply, permeability, filtration performance, etc. Therefore, there is a need to develop a self-powered medical device that is convenient to use, filters particulate matter, and incorporates respiratory monitoring functions to ensure and monitor people's health [123, 124]. Fu et al. designed a self-powered air filter with breathable, efficient filtration of submicron particles (diameter less than 1.0 μm) and respiratory monitoring capability [125]. In the process of respiratory monitoring, synchronous detection signals can be seen on the monitoring appliance by wireless means (Fig. 9g). A conductive metal–organic framework, Ni-HITP, was initially synthesized in-situ on CA aerogel. Subsequently, respiratory-driven triboelectric nanogenerators (R-TENG) were constructed by combining CA/Ni-HITP with a PVDF film. The nanofibers in the PVDF film are stacked in multiple layers, forming massive 3D micro/nanopore structures, and the WCA is as high as 150.9° to prevent water vapor diffusion from affecting

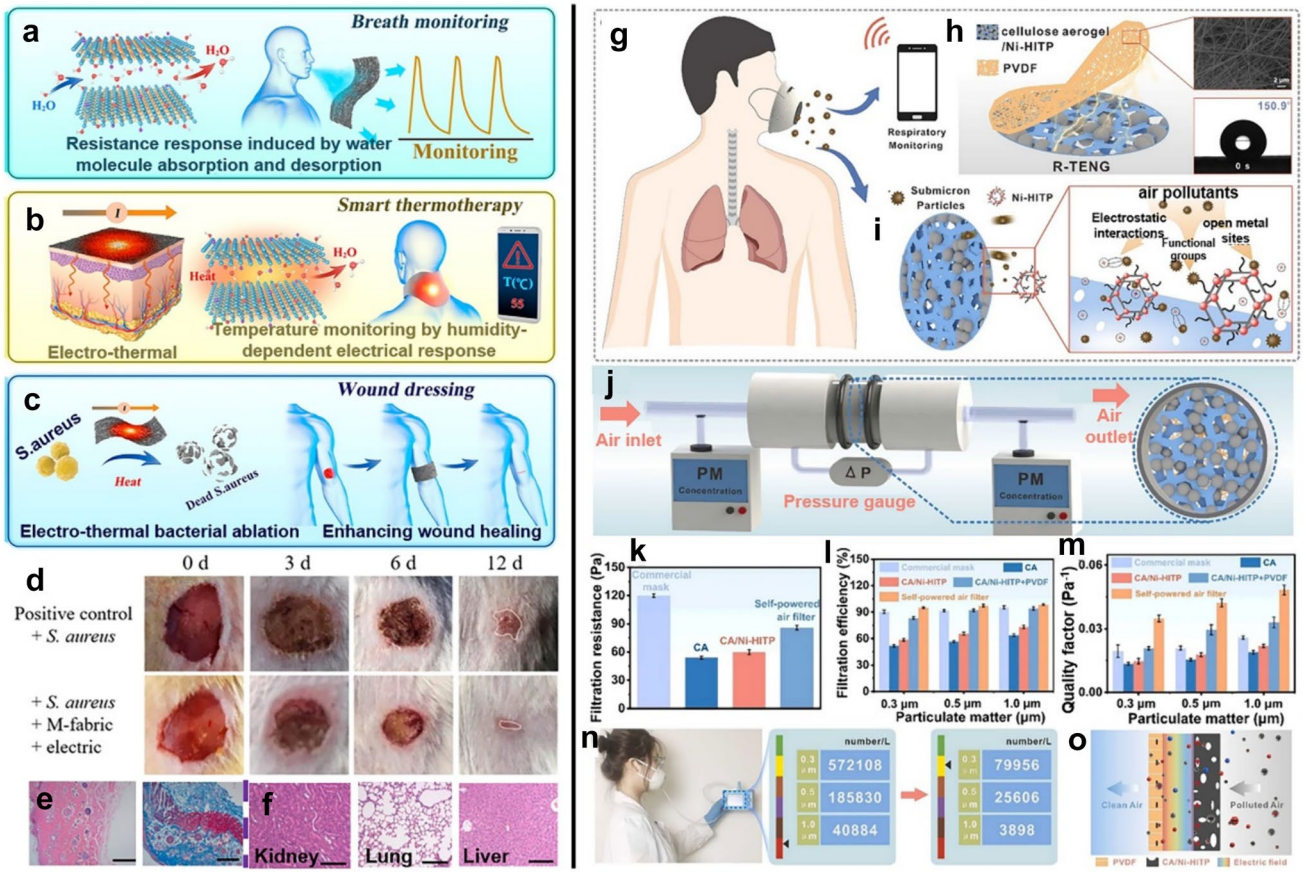

Fig. 9 **a** The humidity response mechanism and respiratory monitoring effect of M-fabric, **b** the intelligent hyperthermia mechanism and temperature monitoring effect of M-fabric, **c** M-fabric ablates bacteria and promotes wound healing under electrical stimulation, **d** digital photographs of the *S. aureus* infected wounds with different treatments, and **e** immunological histological images of skin tissues on rat wounds stained with H&E (left) and Masson (right) after 3 days; reproduced with permission from ref. [120], Copyright 2020, American Chemical Society. **f** H&E staining images of visceral tissue (kidney, lung, and liver) slices of rats after 12 days. **g** Application scenario of the self-powered air filter for respiratory monitoring and removal of submicron particles, and **h** schematic illustration of the structure of R-TENG. The top right and lower right insets show the SEM image and the WCA of PVDF film, respectively, **i** capture mechanism of submicron particles by CA/Ni-HITP, **j** schematic diagram of the device for removing the experiment, **k** comparison of pressure drop across various air filters, **l** comparison of the efficiency of various air filters in removing submicron particles, **m** comparison of QF for removing submicron particles through various air filters, **n** the number of submicron particles outside and inside the mask after wearing for 2 h, and **o** schematic diagram of the filtration mechanism of the self-powered air filter R-TENG; reproduced with permission from ref. [125], Copyright 2022, Elsevier

the CA/Ni-HITP hydrogel layer (Fig. 9h). Based on the traditional physical filtration mechanism and electrostatic adsorption mechanism, the self-powered air filter is further designed (Fig. 9i) [126, 127]. In addition, R-TENG can adsorb and filter submicron particles when CA/Ni-HITP and PVDF films are used as positive and negative triboelectric materials, respectively. The removal efficiency of submicron particles of various sizes produced by burning mosquito coils can be further improved after charging the PVDF film (Fig. 9j). The lower the filter pressure drop (ΔP), the better the air circulation. Loading Ni-HITP on CA aerogel will narrow CA pores, thus increasing the air filtration resistance of CA/Ni-HITP (Fig. 9k). The addition of PVDF film in R-TENG resulted in the increase of ΔP to 86 Pa. However, the ΔP of the cellulose film is lower than 120 Pa than commercial masks, indicating that the cellulose base air filter is more comfortable to wear. R-TENG is endowed with the highest PM removal efficiency compared to other filters in any submicron particulate matter environment (Fig. 9l). Additionally, R-TENG presents the highest quality factor (QF) of filtration capacity for submicron particles with different sizes (Fig. 9m). After operating for 2 h, the content of submicron particles is greatly reduced, and the removal efficiencies of $PM_{0.3}$, $PM_{0.5}$, and $PM_{1.0}$ are 86.0, 86.2, and 90.5%, respectively (Fig. 9n). Electric field was induced by the periodic contact and separation of two substances, which makes the solid air filter partially charged, and the electrostatic gravitational force generated by the electrostatic field

can adsorb tiny charged particles to achieve the effect of air purification (Fig. 9o) [128]. The R-TENG is a self-powered air filter with greater potential applications in removing air pollutants, developing self-powered devices and monitoring human health.

Self-powered sensing systems, capable of harvesting integrated energy and sensing various external physical stimuli, are regarded as pivotal devices in the next generation of smart technologies. This is especially significant given the global population growth and rapid technological advancements in the twenty-first century [129]. Currently, the performance evaluation of electronic devices is usually in laboratory simulation environments, and there is an urgent need to evaluate them in real-world environments in the future to design strategies compatible with real-world applications. Equally importantly, the current manufacturing process for scaleable sustainable electronics is harder to commercialize and industrialize for use, and its mass production still needs to be urgently addressed.

4.3 Electronic Devices

Environmental damage, climate change, air pollution, and a series of ecological objects are all due to the excessive combustion of traditional fossil fuels [78]. The stability of power storage systems can be significantly impacted by the indirectness of environmentally friendly renewable energy sources, such as wind energy, tidal energy, and solar energy, as well as geographical location constraints. Therefore, it is of great significance to manufacture low-cost and environment-friendly high-performance energy storage device materials [130–132]. Nanocellulose can be decomposed into carbon at high temperatures or integrated into other electrochemical active materials to form nitrocellulose-based composite materials. In electrochemical energy storage (EES) systems, it exhibits an extremely hydrophilic surface, numerous layered microporous and mesoporous composite structures for charge storage, and abundant absorption sites that enhance the absorption and transmission of electrolyte ions [133].

Zhang et al. assembled a bifunctional cellulose nanowhisker graphite (CNG) film by the CH–π interaction of graphene (GN) and CNW to alleviate the severe problems of uncontrolled dendritic growth and complex water-induced corrosion of zinc metal anode in AZIBs [134]. Generally, Zn^{2+} coordinates with six water molecules octahedrally to form $[Zn{\cdot}(H_2O)_6]^{2+}$ with high charge density. Zinc anode corrosion and hydrogen evolution reaction (HER) that happened in the process can be attributed to the loss of solvent hindering its diffusion at the electrode interface, resulting in the formation of by-products $Zn_4SO_4(OH)_6{\cdot}5H_2O$ (ZHS) and hydrogen [135, 136]. The deposited CNG film can not only achieve the attraction of CNW to water molecules and the repulsion of GN to water molecules but also prevent $[Zn{\cdot}(H_2O)_6]^{2+}$ from being desolvated under the dual action, thus separating Zn from the electrolyte and preventing anode corrosion of the battery. The negative charge on the surface of CNG films is conducive to the formation of deionization impact, which can allow cations to pass through the CNG film layer, thereby achieving simple migration and uniform deposition of zinc ions. Apart from this, the CNG layer hinders the water corrosion of AZIBs, making its zinc anode strengthen the electrochemical property (Fig. 10a). Under the cyclic operation of the current density at 0.25 mA·h/cm^2, a battery short circuit failure will happen on bare Zn battery, with the polarization voltage increases irreversibly from 65 mV, and the continuous operation time is less than 250 h. In contrast, the polarization voltage of the CNG/Zn battery stabilizes from the initial 42–31 mV and the life span is up to 5500 h. The CNG/Zn battery, due to the above working mechanism, has greatly maintained a stable working state and extended the cycle life of the battery (Fig. 10b). Zn anode-loaded porous nanocellulose matrix composites help to maintain the stability of its structure and reduce the volume change. Acting as a buffer layer, the nanocellulose-based loading layer significantly suppresses hydrogen evolution and zinc corrosion. The cellulosic matrix composite in the Zn cathode is used as the surface coating to protect the cathode from structural degradation and dissolution [137].

Supercapacitors (SC) with high power density and long cycle life have shown great potential in meeting the growing power demand [138–141]. All-solid-state supercapacitors (ASCs) with compactness and leak resistance usually use hydrogel electrolyte, which is composed of a polymer physical framework and injected electrolytic salt/acid/alkali solution [142–144]. To compensate for the mechanical weakness of the hydrogel matrix itself, natural or artificial fibers with unique structural layers are added as reinforcing agents. Twining ultra-fine nanofibers, ranging from 20 to 80 nm, form the porous network structure of the BC [145, 146]. The hydroxy groups in the cellulose chain are in-situ polymerized through hydrogen bonds and electrostatic adsorption, which can easily be assembled into high-strength film materials [147–149].

Li et al. designed a high-performance ASC consisting of a solid-state electrode and a solid electrolyte [150]. The solid-state electrode is composed of polyaniline (PANI) and polyester fiber, as the conductive active substance and the base, respectively [151]. The solid electrolyte was BC nanofiber-reinforced PAM hydrogel. BC/PAM hydrogel fibers can keep their integrity after knotting, indicating the allowance of large deformation and can protect ASC electrodes when subjected to mechanical stress (Fig. 10c). A great deal of tiny spidery BC nanofibers were dispersed in the porous PAM matrix and do not change the original micro-structure of PAM. BC with efficient embedding capabilities can transfer

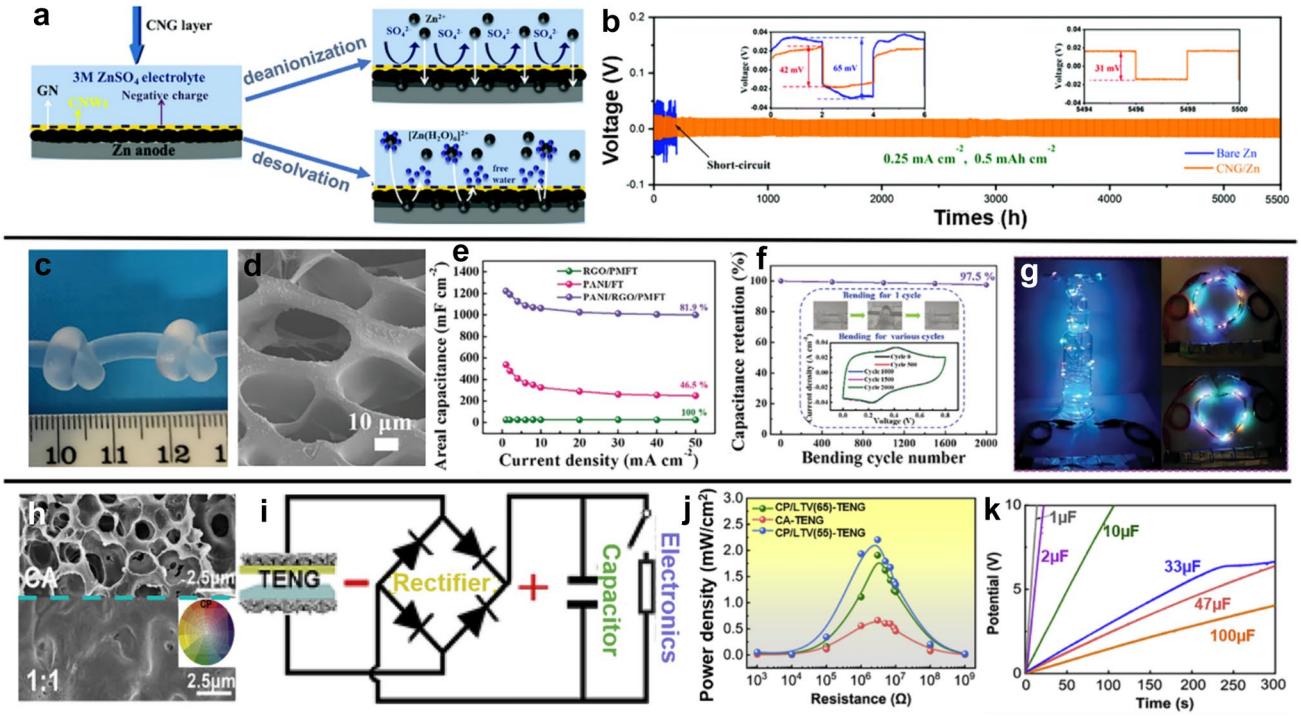

Fig. 10 **a** Schematic diagram of the working mechanism of the CNG layer, **b** comparison of electrochemical performance between bare zinc battery and CNG/Zn battery; reproduced with permission from ref. [134], Copyright 2021, RSC Publishing. **c** Photograph of BC/PAM in the knotted state, **d** SEM image of BC/PAM, **e** the area capacitance under different current densities is calculated by constant current charging and discharging, and **f** cyclic voltammetry curves of the ASC after bending 0, 500, 1000, 1500, and 2000 cycles at 50 mV/s. The illustration is a digital image of the ASC bending cycle, **g** LEDs driven by four-unit ASCs; reproduced with permission from ref. [150], Copyright 2021, Wiley. **h** SEM images of CA and CA/PEI quality ratio of 1:1, with CP digital photo in the inset, **i** the schematic diagram showing the equivalent circuit for charging and discharging, **j** instantaneous power density of different TENG devices at a series of load resistances, and **k** charging curves for different commercial capacitors using the CP-TENG with the area of about 5 cm × 5 cm; reproduced with permission from ref. [162], Copyright 2020, Elsevier

stress from the PAM chain to itself, thereby enhancing mechanical stress (Fig. 10d). During galvanostatic charge/discharge (GCD), the surface capacitance of PANI/RGO/PMFT at 1 mA/cm^2 is 1221 mF/cm^2, and it could be maintained at 1000 mF/cm^2 when the current density increased to 50 mA·cm^{-2}, with the capacitor retention rate up to 81.9%, which proves the high-efficiency performance (Fig. 10e). Furthermore, after thousands of large bending cycles, the CV curve of ASC showed negligible changes and the capacitance retention rate reached 97.5%, which was almost constant, indicating no significant effect on the electrochemical performance of ASC after bending. The porous structure of bulk gel electrolyte can effectively relieve mechanical stress in different deformation processes and avoid relative displacement, thus avoiding the problems of large capacitor interface resistance and slow charge transmission (Fig. 10f). The integrated module of the flexible device can satisfy a variety of practical needs, such as decorative light-emitting diodes (LEDs) (Fig. 10g). The addition of nanocellulose to double-layer capacitor can effectively prevent the aggregation of other component materials, greatly improve the pore utilization in electrode materials [152–154]. Nanocellulose with a high aspect ratio forms a robust entanglement network, enhancing the surface and mechanical properties of the composite electrode, thereby improving the overall electrochemical performance [155].

TENG builds a self-powered system that converts mechanical energy, such as human movement, sound waves, and water currents, into electricity [156]. In 2012, Wang et al. proposed a novel theory of TENG for converting mechanical energy based on Maxwell's displacement current theory, which can transform mechanical energy into electrical energy generated between the two relative polar triboelectric materials through the coupling of electrification and electrostatic induction [157–159]. The degradability, safety, and biocompatibility of cellulosic and its derivatives are compatible with the requirements of environmentally friendly biological materials, providing a prerequisite for the feasibility of cellulosic TENG for wearable electronic devices [160, 161]. Based on the principle of accumulating effective friction charges, Bai et al. prepared porous electroactive and biocomposite film (CP) by physically blending

CA and polyethyleneimine (PEI) and then combined it with flexible silicone rubber to develop high-performance TENG [162]. During the preparation process, the polymer chain was reconfigured, so that the number and size of pores of CP gradually decreased, forming a nested porous structure and producing higher optical transparency (Fig. 10h) [163, 164]. When used as the power, the stable output can ensure the smooth operation of various electronic devices (Fig. 10i). The power density of CP-TENG increases by about 235% compared to that of CA-TENG under the same conditions. This indicates that the porous CP composite can generate and collect more frictional positive charges, thereby increasing its electrical output (Fig. 10j). The CP-TENG accelerates the charging rate at the equivalent charging potential as the capacitance decreases during continuous charging of capacitors with different capacitances, indicating that the electrical energy generated by CP-TENG can be effectively stored in the capacitor (Fig. 10k). Cellulose has low charge affinity and can produce a low triboelectric effect, moreover, studies have shown that CA has higher triboelectric effect than polytetrafluoroethylene (PTFE) [165, 166]. The performance of the cellulose friction layer is close to that of fluoropolymer, which means a higher potential to develop environmentally friendly TENG.

In the era of smart electronics, there is an urgent need for the development of advanced electronic devices that are environmentally friendly, lightweight, flexible, and possess excellent electrochemical properties. Various combinations of cellulose with different types of active materials with high wettability, high mechanical strength, and web-twisted fiber structure can develop electronic devices with excellent performance. However, the design and control of pore structures in cellulose-based electronics are still limited. Reasonable design of pore structures with large specific surface area and multilevel micro- and mesoporous structures is conducive to increasing the contact area between the electrode and the electrolyte, decreasing the diffusion resistance of the electrolyte ions, shortening their diffusion length, and is very favorable to ion transport. Hence, further research efforts are needed to regulate the pore structure of cellulose-based composite electronic devices, paving the way for advancements in future work.

5 Summarization and Prospect

Cellulose-based materials, known for their biocompatibility and degradability, have experienced rapid development across various domains. The green and environmentally conscious development approach has enabled cellulose-based composites to serve as a multi-functional application strategy in numerous fundamental and emerging intelligent fields. This article presents the latest advancements in cellulose materials, focusing on three aspects: the classification of cellulose materials, the properties of cellulose-based materials, and their applications. Additionally, this article provides a comprehensive review of the classification of cellulose and its derivatives based on functional groups and morphology, including MC, CMC, HEC, and CA based on functional group classification, as well as CNC, s-NC, and HTA-CNC based on morphology classification. Furthermore, this discourse delved into the mechanical, antibacterial, gas regulation, hydrophobic, thermal insulation, salt resistance, optical management, and pressure sensitivity properties of materials derived from cellulose. Ultimately, the potential of cellulose-based composites in diverse fields was highlighted. Despite notable advancements in material synthesis and performance enhancement, certain obstacles remain to be overcome in the practical implementation of cellulose-based materials.

5.1 Commercial Large-Scale Preparation of Cellulose Materials

The production of nanocellulose or cellulose with smaller dimensions typically involves the dispersion of cellulose bundles or lengthy cellulose chains through chemical oxidation, assisted by mechanical action. While certain companies have managed to achieve large-scale production of multi-scale cellulose, the efficient and reliable large-scale production of high-quality cellulose with stable physical and chemical properties remains uncertain. In addition, the process of preparing cellulose consumes large amounts of chemicals, such as bleach, and large amounts of energy, such as cooling water and mechanical separation, further limiting its scalability. Furthermore, techniques for the production of cellulose-based materials, such as vacuum filtration, electrospinning, and freeze-drying, are associated with certain limitations, including prolonged processing times, elevated preparation expenses, and reduced efficacy, thereby constraining the practical implementation of such materials. Consequently, the development of green cellulose preparation strategies that are commercial, cost-effective, and energy-efficient on a large scale is imperative.

5.2 Stability and Water Resistance of Cellulose Materials

Cellulose exhibits poor solubility in water owing to the presence of robust intermolecular hydrogen bonds, yet its hydrophilic nature is attributed to the abundance of hydroxy groups in the cellulose chain. The swelling and softening of cellulose upon exposure to water pose significant challenges to its utilization and advancement in various domains. Currently, enhancing the stability of cellulose materials involves

various approaches. These include applying a water-resistant coating on the surface of cellulose through post-treatment, incorporating waterproof additives, or chemically modifying cellulose to be hydrophobic during the pretreatment process, thus improving the water resistance of cellulose-based composites. However, using organic solvents as the reaction medium for hydrophobic treatment can incur significant costs and environmental harm, considering cellulose's inherent hydrophilicity. To align with the principles of green and sustainable cellulose utilization, it is advisable to explore the application of natural hydrophobic materials and conduct the hydrophobic modification process in an eco-friendly manner. To ensure alignment with sustainability and environmental friendliness in cellulose utilization, the adoption of natural hydrophobic materials and the implementation of hydrophobic treatment procedures under solvent-free or water-based conditions may represent the optimal approach to enhance the stability and water resistance of cellulose materials.

5.3 Multi-functional Cellulosic Material Integrated System

Presently, the bulk of cellulose-based materials research is centered on singular functionalities, leading to constrained advancements in the development of integrated multi-functional applications. For instance, the flexible bionic sensor e-skin emulates the human skin's capability to perceive external stimuli, such as temperature, humidity, and pressure, while providing electrical signal feedback. However, with ongoing research, e-skin demands additional features, such as antibacterial properties, self-healing, and health detection. Consequently, to develop more comprehensive and multi-functional cellulose composites, it is imperative to establish a robust cellulose structural system and surface chemistry.

Furthermore, fundamental research is being conducted to investigate the impact of interface engineering on the characteristics of cellulosic materials, and to furnish theoretical direction for the exploration and advancement of multi-functional cellulosic materials. Multidisciplinary fundamental research on the micro-structure of cellulosic materials can be conducted through the utilization of big data processing and computer simulations. This can pave the way for novel, integrated, multi-functional cellulose preparation strategies and cellulose-based material assembly methods. Additionally, it can contribute to the design of advanced and intelligent cellulose-based material structures and functions. Furthermore, this can facilitate the expansion of integrated cellulose-based material systems.

Acknowledgements The authors thank the financial support from the State Key Laboratory for Modification of Chemical Fibers and Polymer Materials (KF2320), National Key Research and Development Program of China (2022YFB3804905, 2022YFB3804900), National Natural Science Foundation of China (22375047 and 22378068 and 22378071), Natural Science Foundation of Fujian Province (2022J01568 and 2020J06038), and State Key Laboratory of New Textile Materials and Advanced Processing Technologies (FZ2021012).

Data availability All the data was used after the permission.

Declarations

Conflict of interest All authors declare that there are no competing interests.

References

1. Jiang F, Li T, Li Y, Zhang Y, Gong A, Dai J, Hitz E, Luo W, Hu L. Wood-based nanotechnologies toward sustainability. *Adv Mater*. **2018**;*30*:1703453.
2. Liu W, Liu K, Du H, Zheng T, Zhang N, Xu T, Pang B, Zhang X, Si C, Zhang K. Cellulose nanopaper: Fabrication, functionalization, and applications. *Nano-Micro Lett*. **2022**;*14*:104.
3. Su Z, Yang Y, Huang Q, Chen R, Ge W, Fang Z, Huang F, Wang X. Designed biomass materials for "green" electronics: A review of materials, fabrications, devices, and perspectives. *Prog Mater Sci*. **2022**;*125*: 100917.
4. Leppänen I, Lappalainen T, Lohtander T, Jonkergouw C, Arola S, Tammelin T. Capturing colloidal nano- and microplastics with plant-based nanocellulose networks. *Nat Commun*. **2022**;*13*:1814.
5. Yeom J, Choe A, Lee J, Kim J, Kim J, Oh SH, Park C, Na S, Shin Y-E, Lee Y, Ro YG, Kwak SK, Ko H. Photosensitive ion channels in layered MXene membranes modified with plasmonic gold nanostars and cellulose nanofibers. *Nat Commun*. **2023**;*14*:359.
6. Yin R, Yang S, Li Q, Zhang S, Liu H, Han J, Liu C, Shen C. Flexible conductive Ag nanowire/cellulose nanofibril hybrid nanopaper for strain and temperature sensing applications. *Sci Bull*. **2020**;*65*:899.
7. Liao SY, Wang XY, Li XM, Wan YJ, Zhao T, Hu YG, Zhu PL, Sun R, Wong CP. Flexible liquid metal/cellulose nanofiber composites film with excellent thermal reliability for highly efficient and broadband EMI shielding. *Chem Eng J*. **2021**;*422*: 129962.
8. Chen F, Xiang W, Sawada D, Bai L, Hummel M, Sixta H, Budtova T. Exploring large ductility in cellulose nanopaper combining high toughness and strength. *ACS Nano*. **2020**;*14*:11150.
9. Zhu W, Droguet B, Shen Q, Zhang Y, Parton TG, Shan X, Parker RM, De Volder MFL, Deng T, Vignolini S, Li T. Structurally colored radiative cooling cellulosic films. *Adv Sci*. **2022**;*9*:2202061.
10. Cho H, Shakil A, Polycarpou AA, Kim S. Enabling selectively tunable mechanical properties of graphene oxide/silk fibroin/cellulose nanocrystal bionanofilms. *ACS Nano*. **2021**;*15*:19546.
11. Isogai A, Zhou Y. Diverse nanocelluloses prepared from TEMPO-oxidized wood cellulose fibers: Nanonetworks, nanofibers, and nanocrystals. *Curr Opin Solid State Mater Sci*. **2019**;*23*:101.
12. Yang W, Pan M, Zhang J, Zhang L, Lin F, Liu X, Huang C, Chen XZ, Wang J, Yan B, Zeng H. A universal strategy for constructing robust and antifouling cellulose nanocrystal coating. *Adv Funct Mater*. **2022**;*32*:2109989.
13. Graham SA, Dudem B, Mule AR, Patnam H, Yu JS. Engineering squandered cotton into eco-benign microarchitectured triboelectric films for sustainable and highly efficient mechanical energy harvesting. *Nano Energy*. **2019**;*61*:505.

14. Li X, Peng Y, Zhang F, Yang Z, Dong Z. Fast-response, no-pretreatment, and robustness air-water/oil amphibious superhydrophilic-superoleophobic surface for oil/water separation and oil-repellent fabrics. *Chem Eng J*. **2022**;*427*: 132043.
15. Liu H, Pang B, Tang Q, Müller M, Zhang H, Dervişoğlu R, Zhang K. Self-assembly of surface-acylated cellulose nanowhiskers and graphene oxide for multiresponsive janus-like films with time-dependent dry-state structures. *Small*. **2020**;*16*:2004922.
16. Sun WB, Han ZM, Yue X, Zhang HY, Yang KP, Liu ZX, Li DH, Zhao YX, Ling ZC, Yang HB, Guan QF, Yu SH. Nacre-inspired bacterial cellulose/mica nanopaper with excellent mechanical and electrical insulating properties by biosynthesis. *Adv Mater*. **2023**;*35*:2300241.
17. Fu J, Wang H, Xiao P, Zeng C, Sun Q, Li H. A high strength, anti-corrosion and sustainable separator for aqueous zinc-based battery by natural bamboo cellulose. *Energy Stor Mater*. **2022**;*48*:191.
18. Wang H, Fu J, Wang C, Wang J, Yang A, Li C, Sun Q, Cui Y, Li H. A binder-free high silicon content flexible anode for Li-ion batteries. *Energy Environ Sci*. **2020**;*13*:848.
19. Osorio M, Posada L, Martínez E, Estrada V, Quintana G, Maldonado ME, Peresin S, Orozco J, Castro C. Bacterial nanocellulose spheres coated with meta acrylic copolymer: Vaccinium meridionale swartz extract delivery for colorectal cancer chemoprevention. *Food Hydrocoll*. **2024**;*147*: 109310.
20. Xu Y, Gao M, Zhang Y, Ning L, Zhao D, Ni Y. Cellulose hollow annular nanoparticles prepared from high-intensity ultrasonic treatment. *ACS Nano*. **2022**;*16*:8928.
21. Wang T, Li S, Tao X, Yan Q, Wang X, Chen Y, Huang F, Li H, Chen X, Bian Z. Fully biodegradable water-soluble triboelectric nanogenerator for human physiological monitoring. *Nano Energy*. **2022**;*93*: 106787.
22. Coughlin ML, Liberman L, Ertem SP, Edmund J, Bates FS, Lodge TP. Methyl cellulose solutions and gels: fibril formation and gelation properties. *Prog Polym Sci*. **2021**;*112*: 101324.
23. Wu Z, Zhang T, Wang B, Ji P, Sheng N, Zhang M, Liang Q, Chen S, Wang H. Scalable bacterial cellulose biofilms with improved ion transport for high osmotic power generation. *Nano Energy*. **2021**;*88*: 106275.
24. Cheng Y, Zhu W, Lu X, Wang C. Lightweight and flexible MXene/carboxymethyl cellulose aerogel for electromagnetic shielding, energy harvest and self-powered sensing. *Nano Energy*. **2022**;*98*: 107229.
25. Xiong J, Li S, Ye Y, Wang J, Qian K, Cui P, Gao D, Lin MF, Chen T, Lee PS. A deformable and highly robust ethyl cellulose transparent conductor with a scalable silver nanowires bundle micromesh. *Adv Mater*. **2018**;*30*:1802803.
26. Cao D, Li Q, Sun X, Wang Y, Zhao X, Cakmak E, Liang W, Anderson A, Ozcan S, Zhu H. Amphipathic binder integrating ultrathin and highly ion-conductive sulfide membrane for cell-level high-energy-density all-solid-state batteries. *Adv Mater*. **2021**;*33*:2105505.
27. Lamanna L, Pace G, Ilic IK, Cataldi P, Viola F, Friuli M, Galli V, Demitri C, Caironi M. Edible cellulose-based conductive composites for triboelectric nanogenerators and supercapacitors. *Nano Energy*. **2023**;*108*: 108168.
28. Dai S, Li X, Jiang C, Zhang Q, Peng B, Ping J, Ying Y. Omnidirectional wind energy harvester for self-powered agro-environmental information sensing. *Nano Energy*. **2022**;*91*: 106686.
29. Angelica NE, Sui X, Ifat KA, Linda JWS, Leitus G, Cohen E, Weissman H, Wagner HD, Rybtchinski B. Modular molecular nanoplastics. *ACS Nano*. **2019**;*13*:11097.
30. Chan CLC, Bay MM, Jacucci G, Vadrucci R, Williams CA, van de Kerkhof GT, Parker RM, Vynck K, Bruno F, Vignolini S. Visual appearance of chiral nematic cellulose-based photonic films: Angular and polarization independent color response with a twist. *Adv Mater*. **2019**;*31*:1905151.
31. Bai L, Jin Y, Shang X, Jin H, Zhou Y, Shi L. Highly synergistic, electromechanical and mechanochromic dual-sensing ionic skin with multiple monitoring, antibacterial, self-healing, and anti-freezing functions. *J Mater Chem A*. **2021**;*9*:23916.
32. Yang K, Chen M, Wang Q, Grebenchuk S, Chen S, Leng X, Novoselov KS, Andreeva DV. Electro-thermo controlled water valve based on 2D graphene–cellulose hydrogels. *Adv Funct Mater*. **2022**;*32*:2201904.
33. Xue JH, Xiang HJ, Zhang YR, Yang J, Cao X, Wang ZL. Characteristic study of self-powered sensors based on native protein composite film. *Energy Environ Mater*. **2023**;*6*: e12492.
34. Jia R, Tian W, Bai H, Zhang J, Wang S, Zhang J. Amine-responsive cellulose-based ratiometric fluorescent materials for real-time and visual detection of shrimp and crab freshness. *Nat Commun*. **2019**;*10*:795.
35. Wang X, Zhang Q, Wang S, Jin C, Zhu B, Su Y, Dong X, Liang J, Lu Z, Zhou L, Li W, Zhu S, Zhu J. Sub-ambient full-color passive radiative cooling under sunlight based on efficient quantum-dot photoluminescence. *Sci Bull*. **2022**;*67*:1874.
36. Zhang X, Cheng Y, You J, Zhang J, Yin C, Zhang J. Ultra-long phosphorescence cellulose with excellent anti-bacterial, water-resistant and ease-to-process performance. *Nat Commun*. **2022**;*13*:1117.
37. Thongsomboon W, Serra DO, Possling A, Hadjineophytou C, Hengge R, Cegelski L. Phosphoethanolamine cellulose: A naturally produced chemically modified cellulose. *Science*. **2018**;*359*:334.
38. Li Z, Zhang Y, Anankanbil S, Guo Z. Applications of nanocellulosic products in food: Manufacturing processes, structural features and multifaceted functionalities. *Trends Food Sci Technol*. **2021**;*113*:277.
39. Fang Z, Li B, Liu Y, Zhu J, Li G, Hou G, Zhou J, Qiu X. Critical role of degree of polymerization of cellulose in super-strong nanocellulose films. *Matter*. **2020**;*2*:1000.
40. Wang J, Niu J, Sawada T, Shao Z, Serizawa T. A bottom-up synthesis of vinyl-cellulose nanosheets and their nanocomposite hydrogels with enhanced strength. *Biomacromol*. **2017**;*18*:4196.
41. Dufresne A. Cellulose nanomaterial reinforced polymer nanocomposites. *Curr Opin Colloid Interface Sci*. **2017**;*29*:1.
42. Liu Y, Lu Y, Zhang H, Liu X, Kong Z, Zhou L, Liu H, Zhang J. Polymer grafting on cellulose nanocrystals initiated by ceric ammonium nitrate: Is it feasible under acid-free conditions? *Green Chem*. **2021**;*23*:8581.
43. Tang J, Sisler J, Grishkewich N, Tam KC. Functionalization of cellulose nanocrystals for advanced applications. *J Colloid Interface Sci*. **2017**;*494*:397.
44. Patel DK, Ganguly K, Dutta SD, Patil TV, Lim KT. Cellulose nanocrystals vs. cellulose nanospheres: A comparative study of cytotoxicity and macrophage polarization potential. *Carbohydr Polym*. **2023**;*303*: 120464.
45. Erdal NB, Hakkarainen M. Degradation of cellulose derivatives in laboratory, man-made, and natural environments. *Biomacromol*. **2022**;*23*:2713.
46. Cheng KC, Catchmark JM, Demirci A. Effects of CMC addition on bacterial cellulose production in a biofilm reactor and its paper sheets analysis. *Biomacromol*. **2011**;*12*:730.
47. Chen HH, Chen LC, Huang HC, Lin SB. In situ modification of bacterial cellulose nanostructure by adding CMC during the growth of Gluconacetobacter xylinus. *Cellulose*. **2011**;*18*:1573.
48. Lin Z, Fu H, Zhang Y, Deng Y, Wei F, Li H, Xu C, Hua F, Lin B. Enhanced antibacterial effect and biodegradation of coating

via dual-in-situ growth based on carboxymethyl cellulose. *Carbohydr Polym*. **2023**;*302*: 120433.
49. Sathishbabu P, Hani U. Development and evaluation of carrier oils encapsulated silver doped zinc oxide nanoparticles loaded bio-plastic composites towards anti-microbial packaging applications. *Inorg Chem Commun*. **2023**;*153*: 110763.
50. Zhang W, Han X, You J, Zhang X, Pei D, Willför S, Li M, Xu C, Li C. Rapid and manual-shaking exfoliation of amidoximated cellulose nanofibrils for a large-capacity filtration capture of uranium. *J Mater Chem A*. **2022**;*10*:7920.
51. Konwar G, Rahi S, Tiwari SP. Decomposable flexible organic transistors with a cellulose-based gate dielectric and substrate for biodegradable electronics. *ACS Appl Mater Interfaces*. **2023**;*15*:35261.
52. Dang C, Shao C, Liu H, Chen Y, Qi H. Cellulose melt processing assisted by small biomass molecule to fabricate recyclable ionogels for versatile stretchable triboelectric nanogenerators. *Nano Energy*. **2021**;*90*: 106619.
53. Saraiva S, Pereira P, Paula CT, Rebelo RC, Coelho JFJ, Serra AC, Fonseca AC. Development of electrospun mats based on hydrophobic hydroxypropyl cellulose derivatives. *Mater Sci Eng C*. **2021**;*131*: 112498.
54. Di Filippo MF, Dolci LS, Liccardo L, Bigi A, Bonvicini F, Gentilomi GA, Passerini N, Panzavolta S, Albertini B. Cellulose derivatives-snail slime films: New disposable eco-friendly materials for food packaging. *Food Hydrocoll*. **2021**;*111*: 106247.
55. Hazarika KK, Konwar A, Borah A, Saikia A, Barman P, Hazarika S. Cellulose nanofiber mediated natural dye based biodegradable bag with freshness indicator for packaging of meat and fish. *Carbohydr Polym*. **2023**;*300*: 120241.
56. Dou J, Karakoç A, Johansson LS, Hietala S, Evtyugin D, Vuorinen T. Mild alkaline separation of fiber bundles from eucalyptus bark and their composites with cellulose acetate butyrate. *Ind Crops Prod*. **2021**;*165*: 113436.
57. Tan HL, Kai D, Pasbakhsh P, Teow SY, Lim YY, Pushpamalar J. Electrospun cellulose acetate butyrate/polyethylene glycol (CAB/PEG) composite nanofibers: A potential scaffold for tissue engineering. *Colloids Surf B*. **2020**;*188*: 110713.
58. Li DH, Han ZM, He Q, Yang KP, Sun WB, Liu HC, Zhao YX, Liu ZX, Zong CN, Yang HB, Guan QF, Yu SH. Ultrastrong, thermally stable, and food-safe seaweed-based structural material for tableware. *Adv Mater*. **2023**;*35*: e2208098.
59. Yang J, Lu X, Zhang Y, Xu J, Yang Y, Zhou Q. A facile ionic liquid approach to prepare cellulose fiber with good mechanical properties directly from corn stalks. *Green Energy Environ*. **2020**;*5*:223.
60. Yang Q, Guo J, Liu Y, Guan F, Song J, Gong X. Improved properties of cellulose/Antarctic krill protein composite fibers with a multiple cross-linking network. *Adv Fiber Mater*. **2022**;*4*:256.
61. Yang H, Liu Z, Yin C, Han Z, Guan Q, Zhao Y, Ling Z, Liu H, Yang K, Sun W, Yu S. Edible, ultrastrong, and microplastic-free bacterial cellulose-based straws by biosynthesis. *Adv Funct Mater*. **2022**;*32*:2111713.
62. Li Z, Chen C, Mi R, Gan W, Dai J, Jiao M, Xie H, Yao Y, Xiao S, Hu L. A strong, tough, and scalable structural material from fast-growing bamboo. *Adv Mater*. **2020**;*32*: e1906308.
63. Scurlock JMO, Dayton DC, Hames B. Bamboo: An overlooked biomass resource? *Biomass Bioenergy*. **2000**;*19*:229.
64. Li Z, Chen C, Xie H, Yao Y, Zhang X, Brozena A, Li J, Ding Y, Zhao X, Hong M, Qiao H, Smith LM, Pan X, Briber R, Shi SQ, Hu L. Sustainable high-strength macrofibres extracted from natural bamboo. *Nat Sustain*. **2021**;*5*:235.
65. Volova TG, Prudnikova SV, Kiselev EG, Nemtsev IV, Vasiliev AD, Kuzmin AP, Shishatskaya EI. Bacterial cellulose (BC) and BC composites: Production and properties. *Nanomaterials*. **2022**;*12*:192.
66. Jawaid M, Chee SS, Asim M, Saba N, Kalia S. Sustainable kenaf/bamboo fibers/clay hybrid nanocomposites: properties, environmental aspects and applications. *J Clean Prod*. **2022**;*330*: 129938.
67. Lin N, Dufresne A. Nanocellulose in biomedicine: Current status and future prospect. *Eur Polym J*. **2014**;*59*:302.
68. Wang Z, Hu W, Wang W, Xiao Y, Chen Y, Wang X. Antibacterial electrospun nanofibrous materials for wound healing. *Adv Fiber Mater*. **2023**;*5*:107.
69. Xie Y, Qiao K, Yue L, Tang T, Zheng Y, Zhu S, Yang H, Fang Z. A self-crosslinking, double-functional group modified bacterial cellulose gel used for antibacterial and healing of infected wound. *Bioact Mater*. **2022**;*17*:248.
70. Liu X, Wu M, Wang M, Hu Q, Liu J, Duan Y, Liu B. Direct synthesis of photosensitizable bacterial cellulose as engineered living material for skin wound repair. *Adv Mater*. **2022**;*34*: e2109010.
71. Abral H, Ariksa J, Mahardika M, Handayani D, Aminah I, Sandrawati N, Pratama AB, Fajri N, Sapuan SM, Ilyas RA. Transparent and antimicrobial cellulose film from ginger nanofiber. *Food Hydrocoll*. **2020**;*98*: 105266.
72. Hu S, Li Y, Peng F, Ou J, Guo L, Chen Y, Li Y, Yue F, Qi H. Plant-inspired modification strategy for the large-scale, versatile preparation of cellulose-based products with highly effective and durable UV-protective, antimicrobial, and antiviral performance. *Chem Eng J*. **2023**;*475*: 146164.
73. Jung S, Cui Y, Barnes M, Satam C, Zhang S, Chowdhury RA, Adumbumkulath A, Sahin O, Miller C, Sajadi SM, Sassi LM, Ji Y, Bennett MR, Yu M, Friguglietti J, Merchant FA, Verduzco R, Roy S, Vajtai R, Meredith JC, Youngblood JP, Koratkar N, Rahman MM, Ajayan PM. Multifunctional bio-nanocomposite coatings for perishable fruits. *Adv Mater*. **2020**;*32*: e1908291.
74. Kim T, Tran TH, Hwang SY, Park J, Oh DX, Kim B-S. Crab-on-a-tree: All biorenewable, optical and radio frequency transparent barrier nanocoating for food packaging. *ACS Nano*. **2019**;*13*:3796.
75. Zhang W, Zhao J, Cai C, Qin Y, Meng X, Liu Y, Nie S. Gas-sensitive cellulosic triboelectric materials for self-powered ammonia sensing. *Adv Sci*. **2022**;*9*: e2203428.
76. Cho S, Yu H, Choi J, Kang H, Park S, Jang J, Hong H, Kim I, Lee S, Jeong HS, Jung H. Continuous meter-scale synthesis of weavable tunicate cellulose/carbon nanotube fibers for high-performance wearable sensors. *ACS Nano*. **2019**;*13*:9332.
77. Yu XF, Li YC, Cheng JB, Liu ZB, Li QZ, Li WZ, Yang X, Xiao B. Monolayer Ti_2CO_2: A promising candidate for NH_3 sensor or capturer with high sensitivity and selectivity. *ACS Appl Mater Interfaces*. **2015**;*7*:13707.
78. Yu X, Yu Z, Zhang X, Li P, Sun B, Gao X, Yan K, Liu H, Duan Y, Gao M, Wang G, Yu S. Highly disordered cobalt oxide nanostructure induced by sulfur incorporation for efficient overall water splitting. *Nano Energy*. **2020**;*71*: 104652.
79. Wang X, Guo J, Ren H, Jin J, He H, Jin P, Wu Z, Zheng Y. Research progress of nanocellulose-based food packaging. *Trends Food Sci Technol*. **2024**;*143*: 104289.
80. Yue C, Wang M, Zhou Z, You Y, Wang G, Wu D. Cellulose-based intelligent packaging films with antibacterial, UV-blocking, and biodegradable properties for shrimp freshness monitoring. *Chem Eng J*. **2024**;*488*: 150975.
81. Ghimire S, Flury M, Scheenstra EJ, Miles CA. Sampling and degradation of biodegradable plastic and paper mulches in field after tillage incorporation. *Sci Total Environ*. **2020**;*703*: 135577.
82. Zhou H, Li Q, Zhang Z, Wang X, Niu H. Recent advances in superhydrophobic and antibacterial cellulose-based fibers and

fabrics: Bio-inspiration, strategies, and applications. *Adv Fiber Mater*. **2023**;*5*:1555.
83. Wang Y, Zhao W, Han M, Guan L, Han L, Hemraj A, Tam KC. Sustainable superhydrophobic surface with tunable nanoscale hydrophilicity for water harvesting applications. *Angew Chem Int Ed*. **2022**;*61*: e202115238.
84. Sun Q, Wang D, Li Y, Zhang J, Ye S, Cui J, Chen L, Wang Z, Butt H-J, Vollmer D, Deng X. Surface charge printing for programmed droplet transport. *Nat Mater*. **2019**;*18*:936.
85. Wang Y, Di J, Wang L, Li X, Wang N, Wang B, Tian Y, Jiang L, Yu J. Infused-liquid-switchable porous nanofibrous membranes for multiphase liquid separation. *Nat Commun*. **2017**;*8*:575.
86. Zhao J, Zhu W, Wang X, Liu L, Yu J, Ding B. Fluorine-free waterborne coating for environmentally friendly, robustly water-resistant, and highly breathable fibrous textiles. *ACS Nano*. **2020**;*14*:1045.
87. Chen K, Li Y, Yang G, Hu S, Shi Z, Yang G. Fabric-based TENG woven with bio-fabricated superhydrophobic bacterial cellulose fiber for energy harvesting and motion detection. *Adv Funct Mater*. **2023**;*33*:2304809.
88. Huang S, Zhang X, Qian X, Ni Y, He Z, Sheng L, Shen J. Rice-leaf-mimetic cellulosic paper as a substrate for rewritable devices and biolubricant-infused "slippery" surfaces. *Chem Eng J*. **2024**;*486*: 150073.
89. Baetens R, Jelle BP, Gustavsen A. Aerogel insulation for building applications: A state-of-the-art review. *Energy Build*. **2011**;*43*:761.
90. Zong D, Zhang X, Yin X, Wang F, Yu J, Zhang S, Ding B. Electrospun fibrous sponges: Principle, fabrication, and applications. *Adv Fiber Mater*. **2022**;*4*:1434.
91. Hou Y, Liao J, Huang L, Guo S, Zhang Y, Liu Z, Mo L, Zhang X, Li J. Plant bio-inspired laminar cellulose-based foam with flame retardant, thermal insulation and excellent mechanical properties. *J Mater Chem A*. **2023**;*11*:1138.
92. Wang H, Zhang R, Yuan D, Xu S, Wang L. Gas foaming guided fabrication of 3D porous plasmonic nanoplatform with broadband absorption, tunable shape, excellent stability, and high photothermal efficiency for solar water purification. *Adv Funct Mater*. **2020**;*30*:2003995.
93. Lin Y, Xu H, Shan X, Di Y, Zhao A, Hu Y, Gan Z. Solar steam generation based on the photothermal effect: From designs to applications, and beyond. *J Mater Chem A*. **2019**;*7*:19203.
94. Chang J, Pang B, Zhang H, Pang K, Zhang M, Yuan J. MXene/cellulose composite cloth for integrated functions (if-cloth) in personal heating and steam generation. *Adv Fiber Mater*. **2024**;*6*:252.
95. Lin X, Wang P, Hong R, Zhu X, Liu Y, Pan X, Qiu X, Qin Y. Fully lignocellulosic biomass-based double-layered porous hydrogel for efficient solar steam generation. *Adv Funct Mater*. **2022**;*32*:2209262.
96. Meng S, Tang CY, Jia J, Yang J, Yang MB, Yang W. A wave-driven piezoelectric solar evaporator for water purification. *Adv Energy Mater*. **2022**;*12*:2200087.
97. Luo B, Wen J, Wang H, Zheng S, Liao R, Chen W, Mahian O, Li X. A biomass-based hydrogel evaporator modified through dynamic regulation of water molecules: Highly efficient and cost-effective. *Energy Environ Mater*. **2022**;*5*:1.
98. Yang H, Jacucci G, Schertel L, Vignolini S. Cellulose-based scattering enhancers for light management applications. *ACS Nano*. **2022**;*16*:7373.
99. Cao X, Hou C, Li Y, Li K, Zhang Q, Wang H. MXenes-based functional fibers and their applications in the intelligent wearable field. *Acta Phys Chim Sin*. **2022**;*38*:2204058.
100. Lee S, An G. Interface engineering of carbon fiber-based electrode for wearable energy storage devices. *Adv Fiber Mater*. **2023**;*5*:1749.
101. Lee B, Oh JY, Cho H, Joo CW, Yoon H, Jeong S, Oh E, Byun J, Kim H, Lee S, Seo J, Park CW, Choi S, Park NM, Kang SY, Hwang CS, Ahn SD, Lee JI, Hong Y. Ultraflexible and transparent electroluminescent skin for real-time and super-resolution imaging of pressure distribution. *Nat Commun*. **2020**;*11*:663.
102. Gong S, Schwalb W, Wang Y, Chen Y, Tang Y, Si J, Shirinzadeh B, Cheng W. A wearable and highly sensitive pressure sensor with ultrathin gold nanowires. *Nat Commun*. **2014**;*5*:3132.
103. Wei Y, Chen S, Lin Y, Yuan X, Liu L. Silver nanowires coated on cotton for flexible pressure sensors. *J Mater Chem C*. **2016**;*4*:935.
104. Zhan Z, Lin R, Tran V, An J, Wei Y, Du H, Tran T, Lu W. Paper/carbon nanotubebased wearable pressure sensor for physiological signal acquisition and soft robotic skin. *ACS Appl Mater Interfaces*. **2017**;*9*:37921.
105. Tao L, Zhang K, Tian H, Liu Y, Wang D, Chen Y, Yang Y, Ren T. Graphene-paper pressure sensor for detecting human motions. *ACS Nano*. **2017**;*11*:8790.
106. Choi H, Sun J, Ren B, Cha S, Lee J, Lee B, Park J, Choi J, Park J. 3D textile structure-induced local strain for a highly amplified piezoresistive performance of carbonized cellulose fabric based pressure sensor for human healthcare monitoring. *Chem Eng J*. **2022**;*450*: 138193.
107. Chen C, Wu Q, Wan Z, Yang Q, Xu Z, Li D, Jin Y, Rojas OJ. Mildly processed chitin used in one-component drinking straws and single use materials: Strength, biodegradability and recyclability. *Chem Eng J*. **2022**;*442*: 136173.
108. Wang X, Pang Z, Chen C, Xia Q, Zhou Y, Jing S, Wang R, Ray U, Gan W, Li C, Chen G, Foster B, Li T, Hu L. All-natural, degradable, rolled-up straws based on cellulose micro- and nano-hybrid fibers. *Adv Funct Mater*. **2020**;*30*:1910417.
109. Kwak H, Kim H, Park SA, Lee M, Jang M, Park SB, Hwang SY, Kim HJ, Jeon H, Koo JM, Park J, Oh DX. Biodegradable, water-resistant, anti-fizzing, polyester nanocellulose composite paper straws. *Adv Sci*. **2022**;*10*: e2205554.
110. Liu J, Wang C, Ewulonu CM, Chen X, Wu M, Huang Y. Fabrication of superhydrophobic and degradable cellulose paper materials for straw application. *Cellulose*. **2021**;*29*:527.
111. Sun P, Wang S, Huang Z, Zhang L, Dong F, Xu X, Liu H. Water-resistant, strong, degradable and recyclable rosin-grafted cellulose composite paper. *Green Chem*. **2022**;*24*:7519.
112. Thanh Uyen NT, Abdul Hamid ZA, Thi LA, Ahmad NB. Synthesis and characterization of curcumin loaded alginate microspheres for drug delivery. *J Drug Deliv Sci Technol*. **2020**;*58*: 101796.
113. Xu XY, Lian X, Hao JN, Zhang C, Yan B. A Double-stimuli-responsive fluorescent center for monitoring of food spoilage based on dye covalently modified EuMOFs: From sensory hydrogels to logic devices. *Adv Mater*. **2017**;*29*:1702298.
114. Gomes V, Pires AS, Mateus N, de Freitas V, Cruz L. Pyranoflavylium-cellulose acetate films and the glycerol effect towards the development of pH-freshness smart label for food packaging. *Food Hydrocoll*. **2022**;*127*: 107501.
115. Widmer S, Dorrestijn M, Camerlo A, Urek SK, Lobnik A, Housecroft CE, Constable EC, Scherer LJ. Coumarin meets fluorescein: A Forster resonance energy transfer enhanced optical ammonia gas sensor. *Analyst*. **2014**;*139*:4335.
116. Xiong Y, Shen Y, Tian L, Hu Y, Zhu P, Sun R, Wong C-P. A flexible, ultra-highly sensitive and stable capacitive pressure sensor with convex microarrays for motion and health monitoring. *Nano Energy*. **2020**;*70*: 104436.
117. Zhu T, Ni Y, Zhao K, Huang J, Cheng Y, Ge M, Park C, Lai Y. A breathable knitted fabric-based smart system with enhanced superhydrophobicity for drowning alarming. *ACS Nano*. **2022**;*16*:18018.

118. Zhang Y, Lu H, Liang X, Zhang M, Liang H, Zhang Y. Silk materials for intelligent fibers and textiles: Potential, progress and future perspective. *Acta Phys Chim Sin*. **2022**;*38*:2103034.
119. Jiang W, Li T, Hussain B, Zhou S, Wang Z, Peng Y, Hu J, Zhang K. Facile fabrication of cotton-based thermoelectric yarns for the construction of textile generator with high performance in human heat harvesting. *Adv Fiber Mater*. **2023**;*5*:1725.
120. Zhao X, Wang LY, Tang CY, Zha XJ, Liu Y, Su BH, Ke K, Bao RY, Yang MB, Yang W. Smart $Ti_3C_2T_x$ MXene fabric with fast humidity response and joule heating for healthcare and medical therapy applications. *ACS Nano*. **2020**;*14*:8793.
121. Ning C, Cheng R, Jiang Y, Sheng F, Yi J, Shen S, Zhang Y, Peng X, Dong K, Wang ZL. Helical fiber strain sensors based on triboelectric nanogenerators for self-powered human respiratory monitoring. *ACS Nano*. **2022**;*16*:2811.
122. Yang Y, Yang Y, Huang J, Li S, Meng Z, Cai W, Lai Y. Electrospun nanocomposite fibrous membranes for sustainable face mask based on triboelectric nanogenerator with high air filtration efficiency. *Adv Fiber Mater*. **2023**;*5*:1505.
123. Zhang H, Yang Y, Su Y, Chen J, Adams K, Lee S, Hu C, Wang ZL. Triboelectric nanogenerator for harvesting vibration energy in full space and as self-powered acceleration sensor. *Adv Funct Mater*. **2014**;*24*:1401.
124. Zhang C, Mo J, Fu Q, Liu Y, Wang S, Nie S. Wood-cellulose-fiber-based functional materials for triboelectric nanogenerators. *Nano Energy*. **2021**;*81*: 105637.
125. Fu Q, Liu Y, Liu T, Mo J, Zhang W, Zhang S, Luo B, Wang J, Qin Y, Wang S, Nie S. Air-permeable cellulosic triboelectric materials for self-powered healthcare products. *Nano Energy*. **2022**;*102*: 107739.
126. Zhang Y, Yuan S, Feng X, Li H, Zhou J, Wang B. Preparation of nanofibrous metal–organic framework filters for efficient air pollution control. *JACS*. **2016**;*138*:5785.
127. Yoo DK, Woo HC, Jhung SH. Removal of particulate matter with metal–organic framework-incorporated materials. *Coord Chem Rev*. **2020**;*422*: 213477.
128. Wang C, Li J, Lv X, Zhang Y, Guo G. Photocatalytic organic pollutants degradation in metal–organic frameworks. *Energy Environ Sci*. **2014**;*7*:2831.
129. Zhu T, Liu L, Huang J, Li S, Lei Y, Cai W, Lai Y, Li H. Multifunctional hydrophobic fabric-based strain sensor for human motion detection and personal thermal management. *J Mater Sci Technol*. **2023**;*138*:108.
130. Admassie S, Ajjan FN, Elfwing A, Inganäs O. Biopolymer hybrid electrodes for scalable electricity storage. *Mater Horiz*. **2016**;*3*:174.
131. Ni Q, Kim B, Wu C, Kang K. Non-electrode components for rechargeable aqueous Zinc batteries: Electrolytes, solid-electrolyte-interphase, current collectors, binders, and separators. *Adv Mater*. **2022**;*34*: e2108206.
132. Zhu X, Jiang X, Liu X, Xiao L, Cao Y. A green route to synthesize low-cost and high-performance hard carbon as promising sodium-ion battery anodes from sorghum stalk waste. *Green Energy Environ*. **2017**;2:310.
133. Wang Z, Lee YH, Kim SW, Seo JY, Lee SY, Nyholm L. Why cellulose-based electrochemical energy storage devices? *Adv Mater*. **2021**;*33*: e2000892.
134. Zhang X, Li J, Liu D, Liu M, Zhou T, Qi K, Shi L, Zhu Y, Qian Y. Ultra-long-life and highly reversible Zn metal anodes enabled by a desolvation and deanionization interface layer. *Energy Environ Sci*. **2021**;*14*:3120.
135. Yuksel R, Buyukcakir O, Seong WK, Ruoff RS. Metal-organic framework integrated anodes for aqueous zinc-ion batteries. *Adv Energy Mater*. **2020**;*10*:1904215.
136. Jia H, Liu K, Lam Y, Tawiah B, Xin JH, Nie W, Jiang S. Fiber-based materials for aqueous zinc ion batteries. *Adv Fiber Mater*. **2023**;*5*:36.
137. Chayambuka K, Mulder G, Danilov DL, Notten PHL. From li-ion batteries toward na-ion chemistries: Challenges and opportunities. *Adv Energy Mater*. **2020**;*10*:2001310.
138. Yan J, Wang Q, Wei T, Fan Z. Recent advances in design and fabrication of electrochemical supercapacitors with high energy densities. *Adv Energy Mater*. **2014**;*4*:1300816.
139. Wang Y, Song Y, Xia Y. Electrochemical capacitors: Mechanism, materials, systems, characterization and applications. *Chem Soc Rev*. **2016**;*45*:5925.
140. Wang F, Wu X, Yuan X, Liu Z, Zhang Y, Fu L, Zhu Y, Zhou Q, Wu Y, Huang W. Latest advances in supercapacitors: from new electrode materials to novel device designs. *Chem Soc Rev*. **2017**;*46*:6816.
141. Guo X, Zhang X, Wang Y, Tian X, Qiao Y. Converting furfural residue wastes to carbon materials for high performance supercapacitor. *Green Energy Environ*. **2022**;*7*:1270.
142. Wang K, Zhang X, Li C, Sun X, Meng Q, Ma Y, Wei Z. Chemically crosslinked hydrogel film leads to integrated flexible supercapacitors with superior performance. *Adv Mater*. **2015**;*27*:7451.
143. Wang Z, Li H, Tang Z, Liu Z, Ruan Z, Ma L, Yang Q, Wang D, Zhi C. Hydrogel electrolytes for flexible aqueous energy storage devices. *Adv Funct Mater*. **2018**;*28*:1804560.
144. Nan J, Zhang G, Zhu T, Wang Z, Wang L, Wang H, Chu F, Wang C, Tang C. A highly elastic and fatigue-resistant natural protein-reinforced hydrogel electrolyte for reversible-compressible quasi-solid-state supercapacitors. *Adv Sci*. **2020**;*7*:2000587.
145. Liu R, Ma L, Niu G, Li X, Li E, Bai Y, Yuan G. Oxygen-deficient bismuth oxide/graphene of ultrahigh capacitance as advanced flexible anode for asymmetric supercapacitors. *Adv Funct Mater*. **2017**;*27*:1701635.
146. Zhang Y, Lin Q, Han J, Han Z, Li T, Kang F, Yang Q, Lü W. Bacterial cellulose-derived three-dimensional carbon current collectors for dendrite-free lithium metal anodes. *Acta Phys Chim Sin*. **2021**;*37*:2008088.
147. Wu ZY, Li C, Liang HW, Chen JF, Yu SH. Ultralight, flexible, and fire-resistant carbon nanofiber aerogels from bacterial cellulose. *Angew Chem Int Ed*. **2013**;*52*:2925.
148. Xu J, Duan L, Liao J, Tang H, Lin J, Zhou X. $KVPO_4F$/carbon nanocomposite with highly accessible active sites and robust chemical bonds for advanced potassium-ion batteries. *Green Energy Environ*. **2023**;*8*:1469.
149. Wang S, Xu Q, Sun H. Functionalization of fiber devices: Materials, preparations and applications. *Adv Fiber Mater*. **2022**;*4*:324.
150. Li X, Yuan L, Liu R, He H, Hao J, Lu Y, Wang Y, Liang G, Yuan G, Guo Z. Engineering textile electrode and bacterial cellulose nanofiber reinforced hydrogel electrolyte to enable high-performance flexible all-solid-state supercapacitors. *Adv Energy Mater*. **2021**;*11*:2003010.
151. Zheng Y, Man Z, Zhang Y, Wu G, Lu W, Chen W. High-performance stretchable supercapacitors based on centrifugal electrospinning-directed hetero-structured graphene–polyaniline hierarchical fabric. *Adv Fiber Mater*. **2023**;*5*:1759.
152. Shao C, Qiu S, Wu G, Cui B, Chu H, Zou Y, Xiang C, Xu F, Sun L. Rambutan-like hierarchically porous carbon microsphere as electrode material for high-performance supercapacitors. *Carbon Energy*. **2020**;*3*:361.
153. Qin H, Liu P, Chen C, Cong HP, Yu SH. A multi-responsive healable supercapacitor. *Nat Commun*. **2021**;*12*:4297.
154. Wu H, Yuan W, Yuan X, Cheng L. Atmosphere-free activation methodology for holey graphene/cellulose nanofiber-based film electrode with highly efficient capacitance performance. *Carbon Energy*. **2022**;*5*: e229.

155. Xu T, Du H, Liu H, Liu W, Zhang X, Si C, Liu P, Zhang K. Advanced nanocellulose-based composites for flexible functional energy storage devices. *Adv Mater*. **2021**;*33*: e2101368.
156. Liu Z, Li H, Shi B, Fan Y, Wang ZL, Li Z. Wearable and implantable triboelectric nanogenerators. *Adv Funct Mater*. **2019**;*29*:1808820.
157. Fan F, Tian Z, Zhong L. Flexible triboelectric generator. *Nano Energy*. **2012**;*1*:328.
158. Wang ZL. On Maxwell's displacement current for energy and sensors: The origin of nanogenerators. *Mater Today*. **2017**;*20*:74.
159. Cai C, Luo B, Liu Y, Fu Q, Liu T, Wang S, Nie S. Advanced triboelectric materials for liquid energy harvesting and emerging application. *Mater Today*. **2022**;*52*:299.
160. Zhao D, Zhu Y, Cheng W, Chen W, Wu Y, Yu H. Cellulose-based flexible functional materials for emerging intelligent electronics. *Adv Mater*. **2021**;*33*: e2000619.
161. Qin Y, Zhang W, Liu Y, Zhao J, Yuan J, Chi M, Meng X, Du G, Cai C, Wang S, Nie S. Cellulosic gel-based triboelectric nanogenerators for energy harvesting and emerging applications. *Nano Energy*. **2023**;*106*: 108079.
162. Bai Z, Xu Y, Zhang Z, Zhu J, Gao C, Zhang Y, Jia H, Guo J. Highly flexible, porous electroactive biocomposite as attractive tribopositive material for advancing high-performance triboelectric nanogenerator. *Nano Energy*. **2020**;*75*: 104884.
163. Asadi Tashvigh A, Chung TS. Facile fabrication of solvent resistant thin film composite membranes by interfacial crosslinking reaction between polyethylenimine and dibromo-p-xylene on polybenzimidazole substrates. *J Membr Sci*. **2018**;*560*:115.
164. Asadi Tashvigh A, Luo L, Chung T-S, Weber M, Maletzko C. Performance enhancement in organic solvent nanofiltration by double crosslinking technique using sulfonated polyphenylsulfone (sPPSU) and polybenzimidazole (PBI). *J Membr Sci*. **2018**;*551*:204.
165. Zou H, Zhang Y, Guo L, Wang P, He X, Dai G, Zheng H, Chen C, Wang AC, Xu C, Wang ZL. Quantifying the triboelectric series. *Nat Commun*. **2019**;*10*:1427.
166. Oh H, Kwak SS, Kim B, Han E, Lim GH, Kim SW, Lim B. Highly conductive ferroelectric cellulose composite papers for efficient triboelectric nanogenerators. *Adv Funct Mater*. **2019**;*29*:1904066.